Yerbilimleri, 2024, 45 (2), 247-273, 1555999

Hacettepe Üniversitesi Yerbilimleri Uygulama ve Araştırma Merkezi Bülteni (*Bulletin of the Earth Sciences Application and Research Centre of Hacettepe University*

YERBİLİMLERİ
Bulletin for Earth Sciences

ISSN: 2687- 2978

Radyonüklid Bakımından Zengin Plaj Kumlarının Mineralojik Bileşiminin Değerlendirilmesi, Geyikli-Çanakkale (Batı Anadolu)

Assessment of mineralogical composition of the natural radionuclide rich beach sands in Geyikli, Çanakkale (Western Anatolia)

FATMA GÜLMEZ [1*], AYDIN YILDIRIM [2], FATMA ŞİŞMAN TÜKEL [3], HATİCE ÜNAL ERCAN [4], YÜKSEL ÖRGÜN TUTAY [1], ZEKİYE KARACIK [1]

[1] Istanbul Technical University, Department of Geological Engineering, İstanbul, Türkiye

[2] Proton Accelerator Facility, Nuclear Energy Research Institute (TENMAK-NUKEN), Ankara, Türkiye

[3] Engineering Faculty, Department of Geological Engineering, Istanbul University-Cerrahpasa, İstanbul, Türkiye

[4] Konya Technical University, Chemistry and Chemical Processing Technologies, Konya, Türkiye, Türkiye

Received *(geliş)*: 23 Eylül (*September*) 2024 Accepted *(kabul):* 20 Kasım (*November*) 2024

ÖZ

Bu çalışma, Batı Anadolu'da Kestanbol plütonunu da bulunduran Miyosen yaşlı Ezine-Ayvacık magmatik kompleksinin kıyısı boyunca uzanan sahilde gözlenen radyonüklid bakımından zengin plaj kumlarının mineralojik bileşimini ele almaktadır. Sahil boyunca radyonüklitlerin plaj kumlarındaki dağılımı düzensizdir. Hantepe plajında en yüksek ^{238}U ve ^{232}Th serisi spesifik aktiviteleri gözlenirken, ^{40}K spesifik aktivitesi orta düzeydedir. Buna karşılık, olasılıkla Kestanbol plütonundan türeyen malzemelerin ağırlıkta olduğu güneydeki plajlarda, Hantepe plajına kıyasla daha yüksek ^{40}K ile daha düşük ^{238}U ve ^{232}Th serisi spesifik aktiviteleri gözlenmektedir.

Bu çalışma kapsamında gama spektrometresi, tüm ve noktasal jeokimya analizleri kullanılmış, kum örneklerinin mineralojik bileşimi ve Kestanbol plütonuna ait felsik damar kayaçları ile nefelin monzogabro ve tefrifonolitik dayklar gibi farklı litolojilerinin radyonüklid konsantrasyonlarının değerlendirilmiştir.

Sonuçlar, Hantepe plajındaki yüksek radyoaktivitenin kaynağının torit grubu mineraller olduğunu ve Kestanbol plütonunun pegmatitik damarlarının, bu minerallerin ana kayacı olduğunu ortaya koymuştur. Bununla birlikte, Miyosen magmatizmasının tüm ürünlerinin farklı seviyelerde radyoelement ve radyonüklid zenginleşmeleri

sergilediği, diğer kayaç yapıcı ve aksesuar minerallerin de potansiyel olarak bölgedeki yüksek doğal arka plan radyasyonuna katkıda bulunduğu değerlendirilmiştir.

Anahtar Kelimeler: Plaser, Doğal Radyoaktivite, Radyonüklit, Kestanbol plütonu, Uranyum, Toryum

ABSTRACT

This study investigates the mineralogical composition of radionuclide-rich beach sands along the coast of the Miocene Ezine-Ayvacık magmatic complex including Kestanbol pluton, in Western Anatolia. The distribution of the radionuclides shows variations along the coast with the highest recorded radioactivity at Hantepe Beach, where specific activities of the ^{238}U-, and ^{232}Th-series are significantly high, while ^{40}K concentrations are moderate. In contrast, the southern beaches, dominated by material from the Kestanbol pluton, have higher ^{40}K concentrations but lower ^{238}U-, and ^{232}Th-series specific activities than Hantepe beach.

Using gamma spectrometry, bulk geochemical, and in-situ analyses, we provide a detailed assessment of the mineralogical composition of the sand samples and the primordial radionuclide concentrations of the different lithologies within the Kestanbol pluton, such as felsic veins, nepheline monzogabbro and tephriphonolitic dykes.

We suggest that thorite group minerals control the high radioactivity at Hantepe beach, and pegmatitic veins of the Kestanbol pluton are the main source rock for thorite minerals. However, all the products of Miocene magmatism in the region exhibit elevated radioelement and radionuclide contents suggesting that other accessory and rock-forming minerals are the potential contributors to the high natural background radiation in the area.

Keywords: *Plaser, Natural Radioactivity, Radionuclides, Kestanbol pluton, Uranium, Thorium*

https://doi.org/10.17824/yerbilimleri.1555999

*Sorumlu Yazar/ Corresponding Author: gulmezf@itu.edu.tr

INTRODUCTION

Beaches are high-energy depositional environments where weathered and eroded materials from source rocks are transported, sorted, and deposited by the action of a variety of forces, such as waves, winds, longshore currents and tides. These processes not only shape the coastal landscape but also lead to the formation of laminated or lens-shaped economic mineral deposits, in some cases, including placers that may contain elevated levels of primordial radionuclides (Hou et al., 2017). Such placers, like those found along the coasts of Brazil, India and Egypt, are typically associated with specific heavy minerals, including allanite, xenotime, thorite, monazite, zircon, and sphene (UNSCEAR Report, 2000). These types of placers have been extensively investigated for their economic potential, particularly for Rare Earth Elements (REE), environmental radiation exposure, and geological insights into source rock characteristics. However, the understanding of such deposits remains incomplete, particularly in regions with complex geological histories such as Western Anatolia.

Hantepe beach, located near Geyikli, is one of the high natural background radiation areas at the northern Aegean coast with Mykonos, Naxos and Touzla (Filippidis et al. 1997; Örgün et al., 2007; Çetiner et al., 2011; Papadopoulos et al., 2014; 2015; 2016). Furthermore, it has been demonstrated that this beach exhibits, the highest mean activity concentration and dose rates in comparison with the other beaches surrounding the Anatolia Peninsula (Table 1). The results of the spectroscopic analysis of beach sands and nearby rocks revealed that the high natural background radiation primarily originates from Kestanbol pluton (Örgün et al.,

2007; Cetiner et al., 2011, 2012), a uranium-rich granitoid that has also been recently identified as a significant contributor to the high regional heat flow (Chandrasekharam and Baba, 2021). Similarly, the Kestanbol pluton is among the most radiogenic magmatic bodies in the northern Aegean region, in a manner comparable to the Oligo-Miocene plutons in Greece and Western Anatolia (Örgün et al., 2007). These include those found in the Rhodope, Serbomacedonian massifs, Pelagonian zone and Sakarya Zone (Papadoupoulas et al., 2014, 2017; Karadeniz and Akal, 2014; Angı et al., 2017). However, the Kestanbol pluton is a complex magmatic body with various lithologies (Karacık and Yılmaz, 1998; Şahin et al., 2012; Akal, 2012, Öztürk et al., 2020). Consequently, it cannot be considered as the sole contributor to the observed high natural background radiation. However, the lack of further lithological or mineralogical descriptions in previous gamma spectrometry studies, aside from location information, has resulted in uncertainty regarding the type and the exact source of the radiogenic minerals.

Furthermore, the distribution of radioactivity along the coastline, running parallel to the pluton's west border, shows significant variability, with Hantepe beach exhibiting the highest total and ^{232}Th specific activities despite its relative distance from the pluton (Figure 1). Some specific lithologies, such as ultrapotassic and potassic dykes previously classified as the mafic dykes of the Kestanbol pluton, have high U and Th contents (Örgün et al., 2007; Şahin et al., 2012; Akal, 2012, Öztürk et al., 2020). These lithologies, have been proposed to explain radioactivity anomalies, due to their relatively high concentrations of radioelement and ∑REE, assuming that monazite, apatite, zircon and thorite are common to beach sands and these rocks, without in-depth mineralogical investigations (Unluer et al., 2021, Döner et al., 2022). To address the uncertainties regarding mineralogical composition of the sand samples from Hantepe beach and nearby beaches, Odunluk and Akliman, and of their source rocks, we have investigated the sand fractions by combining gamma spectrometry analysis with in-situ and bulk geochemical analysis. We have also performed gamma spectrometry and bulk geochemical analysis on the rock samples representing the mafic and felsic dykes and stocks of the Kestanbol pluton. We report, for the first time, the lithology-dependent radionuclide concentrations of the magmatic rocks and the presence of thorite group minerals in the beach sands, providing a comprehensive insight into the sources of natural radioactivity in the region.

GEOLOGICAL BACKGROUND

The Biga Peninsula in northwest Anatolia present a complex tectonic landscape of amalgamated oceanic and continental fragments, extensively overlain by Tertiary magmatic activity, which produced a range of plutonic and volcanic formations. The pre-Tertiary tectonic history of the area is a topic of considerable debate, but its magmatism is relatively well understood (Okay et al., 1991, Okay and Satır, 2000; Beccaletto ve Jenny, 2004, Okay and Goncüoğlu, 2004; Duru et al., 2012, Aygül et al., 2012; Yiğitbaş and Tunç 2020). Magmatism began with the emplacement of middle Eocene plutons in the northern parts of the peninsula, subsequently migrted southward, forming the Kestanbol, Evciler, Eybek, Yenice, and Kazdağ plutons, accompanied by the Oligo-Miocene volcanism and core-complex exhumation (Karacık and Yılmaz, 1998; Aldanmaz et al., 2000; Altunkaynak et al., 2012; Black et al., 2013; Aysal, 2015; Öztürk et al., 2020). These magmatic associations are unconformably overlain by shallow marine carbonates and

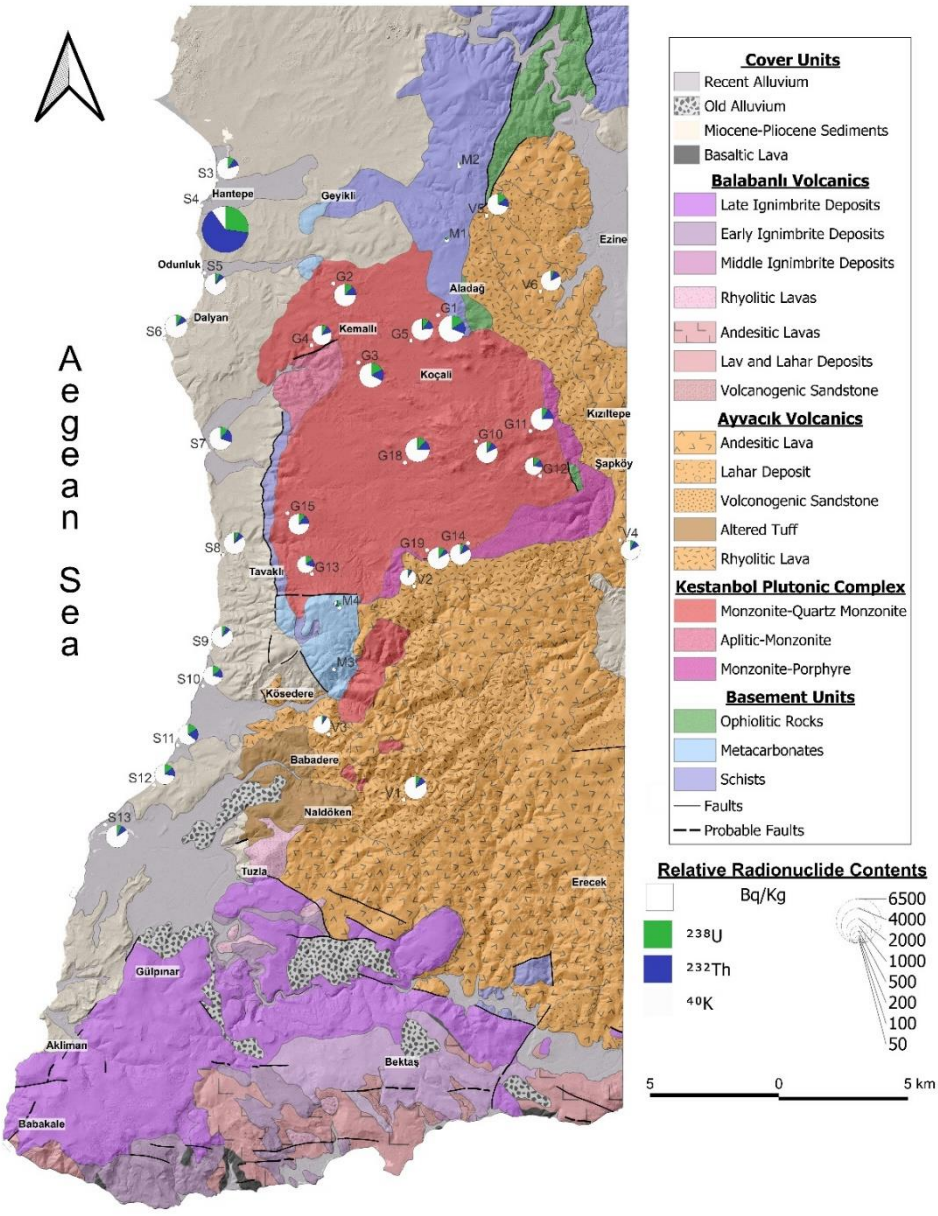

Figure 1. Geologic map of SW Biga Peninsula and its surroundings is adapted from Karacık (1995). Map of basement rocks to the north of Aladağ is from Yiğitbaş and Tunç (2020). Radionuclide contents of representative samples of beach sand (S), plutonic/hypabyssal (G) and volcanic (V) rocks compiled from Örgün et al. (2007) to show the relative contents of primordial radionuclides (^{238}U and ^{232}Th series and ^{40}K). Pie charts, with radii proportional to the total radionuclide content of each sample, were generated using QGIS.org (3.34.6).

Şekil 1. *Biga Yarımadası'nın güneydoğusunun jeoloji haritası Karacık'tan (1995) uyarlanmıştır. Aladağ'ın kuzeyinde metamorfik temel kayaların dağılımları Yiğitbaş ve Tunç'tan (2020) alınmıştır. Plaj kumları (S), plütonik/hipabisal (G) ve volkanik (V) kayaların doğal radyonüklit (^{238}U ve ^{232}Th serisi ile ^{40}K) içerikleri Örgün vd.'nden (2007) derlenmiştir. Örneklerde doğal radyonüklidlerin oransal dağılımlarını gösteren ve yarıçapları toplam radyonüklit içeriği ile orantılı olan pasta grafikler QGIS.org (3.34.6) ile hazırlanmıştır.*

Table 1. The mean specific activity concentrations (Bq kg^{-1}) of primordial radionuclides (^{238}U series, ^{232}Th series, and ^{40}K) and the range of dose rate (μGy/h) were measured in the beach sands of Anatolia and in some of the high natural background areas around the world (1: Çetiner et al. 2012; 2: Özden and Aközcan, 2021; 3: Kapdan et al., 2012; 4: Kucukomeroglu et al., 2016; 5: Kucukomeroglu et al., 2016; 6: Kucukomeroglu et al., 2016; 7: Aytekin et al., 2015; 8: Yalcin and Unal, 2018; 9: Taşköprü et al., 2024; 10: Unal et al., 2024; 11: Papadopoulas et al., 2014;, 12: Papadopoulas et al., 2015; 13: Papadopoulas et al., 2016; 14: Papadopoulas et al., 2016; 15: Veiga et al., 2006; 15: UNSCEAR Report, 2000; 17: Mohanty et al., 2004).

Tablo 1. *Dünya geneinde bazı yüksek doğal arka plan radyasyonu alanları ile Anadolu'da çeşitli plajlarda ölçülmüş doğal radyonüklitlerin (^{238}U serisi, ^{232}Th serisi ve ^{40}K) ortalama aktivite konsantrasyonları ve doz hızı aralığı (1: Çetiner vd. 2012; 2: Özden ve Aközcan, 2021; 3: Kapdan vd., 2012; 4: Kucukomeroglu vd., 2016; 5: Kucukomeroglu vd., 2016; 6: Kucukomeroglu vd., 2016; 7: Aytekin vd., 2015; 8: Yalcin ve Unal 2018, 9: Taşköprü vd., 2024; 10: Unal vd., 2024; 11: Papadopoulas vd., 2014; 12: Papadopoulas vd., 2015; 13: Papadopoulas vd., 2016; 14: Papadopoulas vd., 2016; 15: Veiga vd., 2006;15: UNSCEAR Raporu, 2000; 17: Mohanty vd., 2004).*

	Mean Specific Activity (Bq kg^{-1})			Dose Rate (μ Gy h^{-1})	Reference
Location	^{238}U	^{232}Th	^{40}K		
Hantepe Beach, Çanakkale	3616.0	12096.7	1364.3	0.00-10.1	[1]
Aliağa, İzmir	-	50.2	721.3	0.05-0.10	[2]
Kapıdağ, Balıkesir	16.5	67.1	569.2	0.02-0.29	[3]
Trabzon	12.0	7.0	224.0	0.00-0.05	[4]
Giresun	21.0	14.0	531.0	0.00-0.07	[4]
Ordu	24.0	11.0	645.0	0.00-0.11	[4]
Zonguldak	23.2	20.0	244.8	-	[5]
Kumluca, Antalya	68.0	38.0	341.0	0.01-0.12	[6]
Lara, Antalya	11.9	9.8	238.1	0.01- 0.04	[7]
Cleopatra and Damlataş, Antalya	-	24.0	276.9	0.00-0.07	[8]
Sarti and Sykia, Chalkidiki	61.0	140.2	496.2	0.03-0.28	[9]
Aspri Ammos, Kavala, Nea Peramos, Ag Marina, Eleoxori, Kavala	323.4	1211.9	661.9	0.06-3.01	[10]
Naxos Island	199.0	601.8	433.3	0.04-1.25	[11]
Mykonos Island	127.6	1276.0	995.4	0.07-6.46	[11]
Guarapari, Brazil	-	55537.0	63.0	0.09-90.0	[12, 13]
Orissa, India	350.0	2825.0	180.0	0.64-3.09	[14]
Earth's Average	33	45	420	0.06	[13]

continental clastics, and the magmatic activity diminished by the Late Miocene-Pliocene, producing mainly alkali basaltic lavas (Aldanmaz, 2000; Aysal et al., 2015). Miocene magmatism has left a significant imprint on the regions around Ezine and Ayvacık, where radionuclide-rich sands are found. This magmatism is exemplified by the Kestanbol pluton, the Ayvacık volcanic assemblage to the east and south of the pluton, and the Balabanlı volcanic assemblage, which is exposed between Gülpınar, Babakale, and Behramkale (Karacık, 1995). The beaches hosting radioactive placers are bordered by pre-Tertiary basement rocks, Miocene magmatic association and Late Miocene-Pliocene sedimentary cover units. Since basement and cover units have negligible radionuclide concentrations, this study focusses on the magmatic association which is the primary source of radionuclide enrichment in the beach sands.

Basement Rocks

The pre-Tertiary basement of the Biga Peninsula considered to be associated with various tectonic units such as Kazdağ Massif, Sakarya Continent, Rhodope Zone, Karakaya Complex, and Intra-Pontid Suture (Okay et al., 1991; Okay and Satır, 2000; Beccaletto and Jenny, 2004; Okay and Goncüoğlu, 2004; Duru et al., 2012; Aygül et al., 2012; Yiğitbaş and Tunç 2020). In the vicinity of the radioactive placer beaches, the basement, so-called “Ezine zone”, consisting of metamorphic (Karadağ group and Çamlıca massif) and ophiolitic (Denizgören ophiolite) units (Okay et al., 1990; Duru et al., 2012; Yiğitbaş and Tunç 2020). The metamorphic units form a narrow belt along the coast between Kestanbol in the north and Kösedere, with broader outcrops northeast Geyikli, overlain by Cretaceous ophiolite. The lower part of the metamorphic succession is represented by low-grade metaclastic and metacarbonate sequence (Duru et al., 2012, Yiğitbaş and Tunç 2020).

Metaclastic units consist of varying amounts of quartz, muscovite, chlorite, epidote and calcite and accessory tourmaline (Karacık, 1995; Yiğitbaş and Tunç, 2020). The upper part of the succession is made up of a metacarbonate sequence containing massive recrystallised and laminated clay rich limestones and conglomerates (Duru et al., 2012).

The uppermost part of the Ezine Zone is represented by Denizgören ophiolite which consists of harzburgite and sporadic gabbro with diabase-type ultramafic and ultrabasic rocks that affected by extensive serpentinization. The ophiolitic units have limited outcrops around the Kestanbol pluton, but from Karadağ to northwards, they form a 2-3 km wide and 10 km long tectonic slice. The primary mineralogical composition has changed due to the serpentinization, the veins filled with secondary epidote and albite.

Magmatic Association

Magmatic association in the region comprises a pluton of quartz monzonitic-granodioritic composition, named Kestanbol pluton with coeval lava- and pyroclastic -dominated volcanics known as Ezine and Balabanlı volcanic successions respectively (Figure 1). Isotopic age analysis suggests that the magmatic association developed in Early Miocene (Kestanbol pluton: 22.43 ± 0.26 - 22.10 ± 0.25 Ma, Ezine volcanics: 21.83 ± 0.21 Ma, Balabanlı volcanics: 19.38 ± 0.18 Ma; Öztürk et al., 2020 and references therein).

Kestanbol Pluton

The Kestanbol Pluton outcrops over an area of about 140 km^2 between Ezine and Geyikli and Kösedere. It is bordered to the north and north-east predominantly by metamorphic basement rocks and to the north-east by ophiolitic rocks. The pluton has a transitional contact with altered felsic lavas and tuffs via its hypabyssal equivalent, the Poruklu Formation. It also has a contact, an aurole defined by hornblende- and

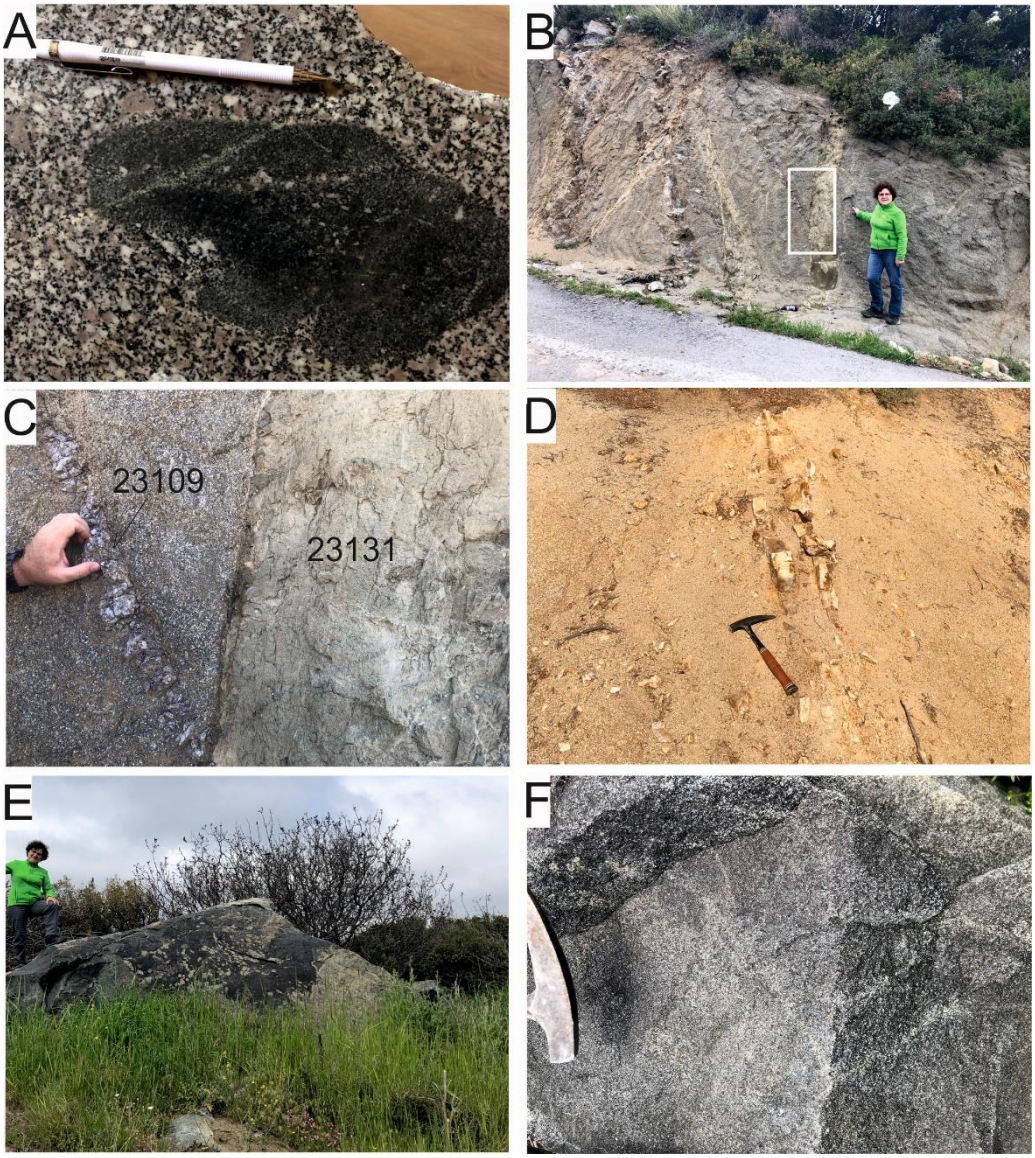

Figure 2. Field photos of the enclaves, felsic and mafic dykes of the Kestanbol pluton, a) mafic microgranuler enclave, b) monzonitic country rock crosscut by mafic dykes and pegmatitic veins, c) close-up view of the crosscutting relations ship between mafic dyke and pegmatitic vein, d) aplitic dykes within weathered monzonitic country rock, e) general view of the nepheline monzogabbro block, f) close-up view of the nepheline monzogabbro with dark, massive and granular texture.

Şekil 2. *Kestanbol pütonuna ait anklavlar ile mafik ve felsik dayklarını gösteren saha fotoğrafları, a) mafik mikrogranüler anklav, b) monzoniti kesen mafik dayklar ile pegmatitik damarlar, c) pegmatitik damarı kesen mafik daykın yakından görünümü, d) ayrışmış monzonitler içinde aplit dayklarını, e) nefelin monzogabro blokunun genel görünümü, f) koyu renkli, masif ve granüler dokulu nefelin monzogabronun yakından görünümü.*

pyroxene-hornfels with an aplitic zone (the chilled margin) along its western boundary with metamorphic basement rocks (Karacık and Yılmaz, 1998). The pluton contains mafic microgranular enclaves and cut by a set of dykes and veins revealing ultrapotassic, latitic, pegmatitic and aplitic compositions (Figure 2a-f; Karacık and Yılmaz, 1998; Şahin et al., 2010; Akal, 2013).

The outcrops of the Kestanbol Pluton are characterized by rounded, massive boulders with minimal jointing, a distinctive feature of the northern exposures. In various locations, the plutonic rocks exhibit an arena-like appearance, indicative of extensive weathering. These rocks are holocrystalline with coarse to medium grains of alkali feldspar, plagioclase, quartz, biotite, amphibole with accidental clinopyroxene, in varying proportions (Figure 3a-b). They are classified as monzonite, quartz monzonite syenite and granite based on their mineralogical composition by different studies. According to Andaç (1973, 1975), the earliest study investigating the geological background of the high natural background radiation in the region, accessory minerals in the plutonic rocks are sphene, zircon, allanite, apatite, epidote, thorite, uranothorite (% 0.1–4.5). Notably, sphene, the most abundant accessory mineral, occasionally challenging its classification as an accessory phase with a modal proportion above 1%, can locally form anhedral grains up to 0.5 mm (Figure 3a). The Poruklu formation, hypabyssal equivalent of the pluton, share identical mineralogical composition but display porphyritic textures (Figure 3c). However, no findings of radiogenic accessory phases have been reported from these rocks, to our knowledge. The chilled margin of the pluton extending to the east, defined as aplogranitic rocks (Karacik and Yilmaz, 1998) reveal a fine-grained granular and perthitic texture with a feldspar-dominated mineralogy. Disseminated enclaves within the pluton are abundant and classified as monzonite, diorite and their quartz-bearing variations (Şahin et al., 2010). They are holocrystalline, fine grained and more enriched with hypidiomorphic mafic minerals resulting in a darker colour when compared to their host but their mineralogical compositions are comparable (Figure 3d). They are consisting of plagioclase, hornblende, biotite, K-feldspar, quartz, pyroxene and sphene, apatite, epidote with oxide minerals as accessory phases (Şahin et al., 2010).

The veins and dykes cutting through the pluton are diverse including pegmatite, aplite, latite porphyre/micromonzonite, lamprophyre and leucite porphyry classified under the felsic and mafic dyke groups by Şahin et al. (2010). Aplitic, pegmatitic and granophyric dykes exhibiting sharp contacts with the country rocks (Figure 2a-b). These rocks vary in grain size, with pegmatites containing K-feldspar megacrysts whle aplitic and granophyric types are generally fine- to medium-grained, equigranular, and locally porphyritic. Andaç (1975) identified uranothorite and thorite inclusions along with magnetite, sphene, apatite and zircon within the hornblendes in some of the aplitic veins to the north of the Kestanbol pluton around Aladağ, which correlated with the local anomalies in radioactivity. During our field studies, we identified radiogenic veins and dykes in a road cut between Kemallı and Geyikli, characterized by a purplish-pink colour, medium to coarse grain size and thicknesses of 15-20 cm for the vein and 30-50 cm for the dyke. The vein, consisting of green, dull and prismatic crystals of ~0.5 mm in some parts, is cut by one of the mafic dykes of the Kestanbol pluton (Figure 2b-c). Petrographic studies on the representative samples suggest that the rock can be classified as a K-feldspar pegmatite consisting perthitic K-feldspar, plagioclase with minor amphibole and occasional clinopyroxene (Figure 4a-d). Carbonate minerals display sharp boundaries with feldspars and may include acicular

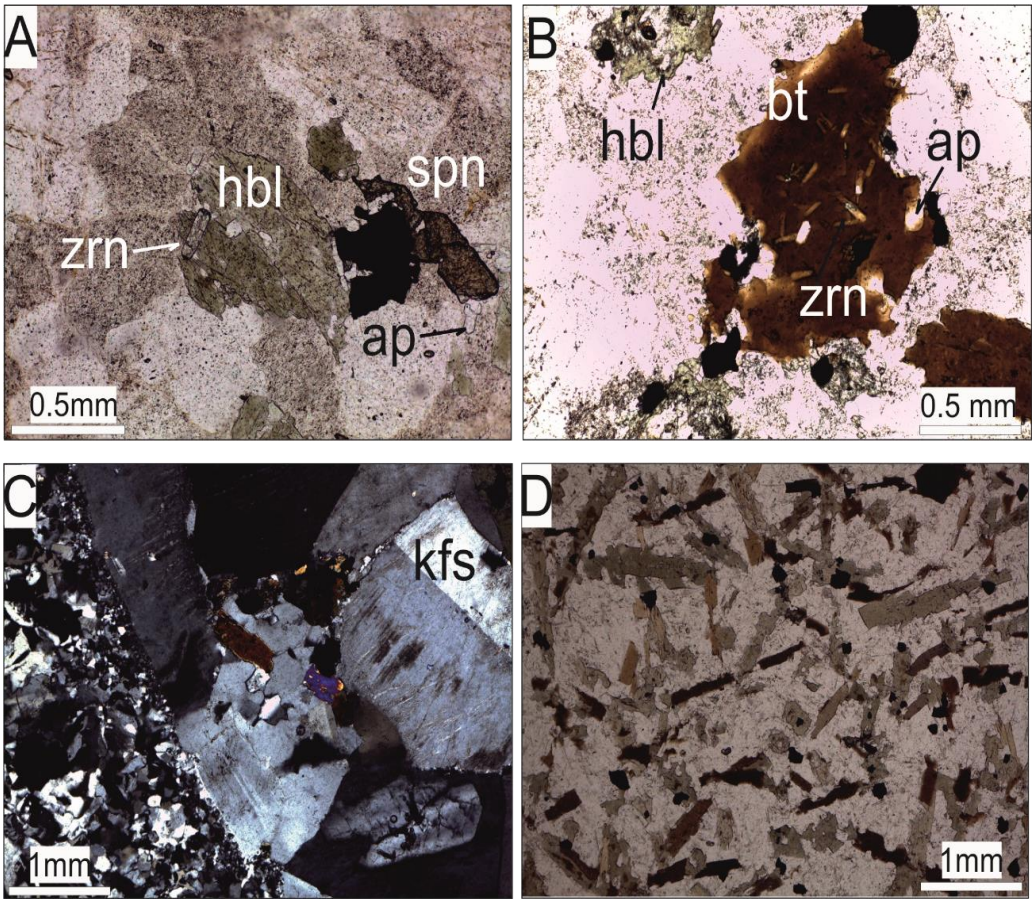

Figure 3. Micro-photographs of the samples representing plutone and its transitional contact (Poruklu formation) with mafic microgranular enclaves, a) plane polarized light view of holocrystalline medium grained monzonite with hypidiomorphic hornblende (hbl), feldspar phenocrystals, sphene microphenocrystal with zircon and apatite microcrystals, b) plane polarized light view of monzonitic sample with anhedral biotite (bt) phenocrystals with acicular zircon (zrn) and apatite (ap) inclusions, c) cross polarized light view of monzonite porphyre (Poruklu formation) with porphyritic texture due to the phenocrystals and microcrystals of K-feldspar (kfs), d) plane polarized light view of mafic microgranular enclave with abundant biotite and plagioclase crystals displaying inequigranular, hypidiomorphic textures.

Şekil 3. *Plütonu, plütonun geçiş zonu (Poruklu Formasyonu) ve mafik mikrogranülar anklavlarını temsil eden örneklerin mikrofotoğrafları a) holokristalen orta taneli monzonitlerde hipidiyomorfik hornblend (hbl) ve feldispat fenokristalleri, sfen mikrofenokistallari ve zirkon, apatit mikrokristallerinin doğal ışıkta görünümü, b) monzonitte iğnemsi zirkon ve apatit kapanımları bulunduran anhedral biyotitin (bt) doğal ışıkta görünümü, c) monzonit porfirde (Poruklu formasyonu) K-feldispat fenokristal ve mikrokristallerine bağlı porfirik dokunun polarize ışıkta görünümü, d) hipidiyomorfik dokulu, biyotit ve plajiyoklas bulunduran mafik mikrogranüler anklavların doğal ışıkta genel görünümü*

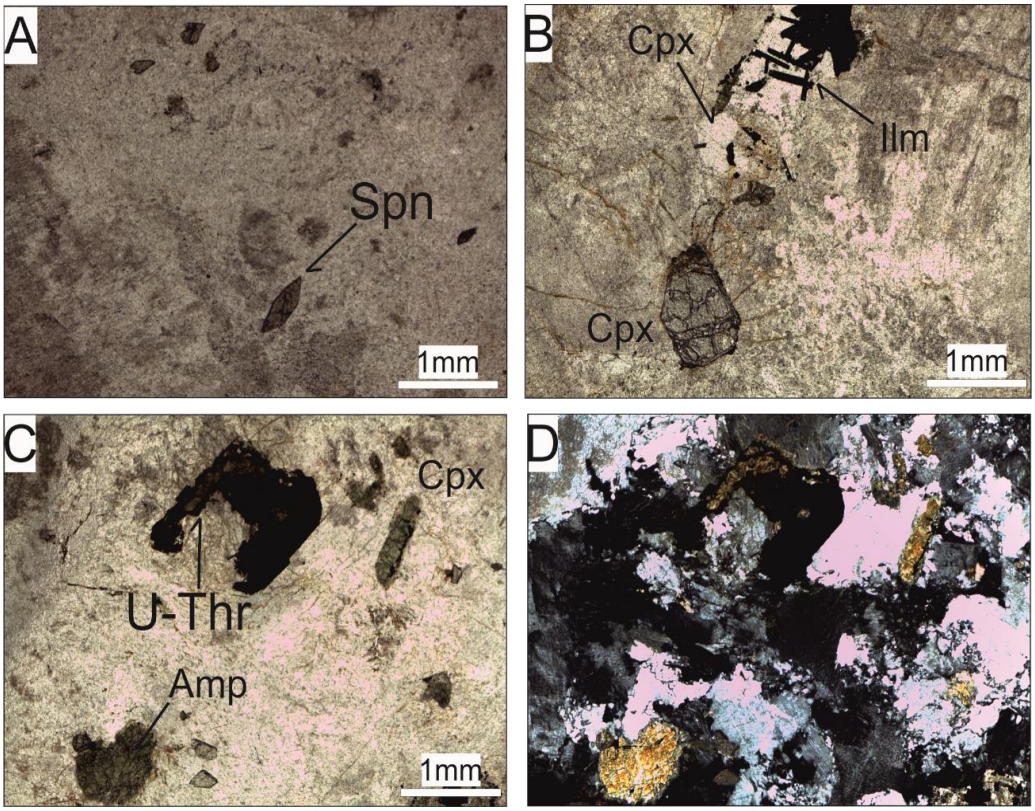

Figure 4. Micro-photographs of a representative sample from the most radiogenic pegmatitic vein, one of the felsic dyke type in the Kestanbol pluton, a) altered feldspars characterized by an earthy appearance and idiomorphic sphene (Spn) crystals (plane polarized light), b) acicular ilmenite crystals in secondary carbonates alongside an idiomorphic clinopyroxene phenocrystal (plane polarized light) c) plane polarized light view of the sample showing partly opaque uranothorite (U-Thr) crystal and altered amphibole (amp) crystals, d) cross polarized light view of the same area, revealing the microperthitic texture.

Şekil 4. *Kestanbol plütonuna ait felsik dayklardan, radyojenik pegmatitik damara ait temsilci örneklerin mikro-fotoğrafları, a) toprağımsı görünüm ile tipik alkali feldispat ve idiyomorfik sfen (Spn) kristallerinin görünümü (doğal ışık), b) idiyomorfik klinopiroksen fenokristali ile ikincil karbonatlar içinde asiküler ilmenit kristalleri (doğal ışık) c) kısmen opaklaşmış uranotorit (U-Thr) kristali ve altere amfibol (amp) kristalleri (doğal ışık), d) aynı alanın polarize ışık altında görünümü mikropertititk dokuyu ortaya çıkarmaktadır.*

ilmenite and other opaque minerals (Figure 4b). The green prismatic minerals identified by in-situ analysis as uranothorite micro- and pheno-crystals, are partlially opaque and have a reddish birefringence (Figure 4c-d). Sphene is the most abundant accessory mineral accompanied by apatite.

Previously described as lamprophyres and leucite-porphyry (Şahin et al., 2010), the mafic dykes, are of ultrapotassic/shoshonitic composition. Their nomenclature was updated by Akal (2012) as the leucite-aphyric and leucite-phyric tephriphonolite dykes. Outcrops are well-exposed on road cuts near Geyikli and Kemallı. The leucite-aphyric dykes, 30-50 cm thick, have sharp contact with the plutonic rocks into which they have intruded, dark in

colour and earthy in appearance. They have fine grained porphyritic textures with extensively altered phenocrystals of biotite and plagioclase replaced by chlorite and a mixture of sericite and epidote respectively (Figure 5a-b). The groundmass is aphanitic with micro-crystals of clinopyroxene, biotite, K-feldspar and plagioclase that were replaced by secondary minerals due to extensively alteration.

The leucite-phyric variety is characterized by the porphyritic textures with white, large and euhedral leucite phenocrystals (up to 1.5 cm) in a black matrix. Unlike the leucite-aphyric variety they have irregular, lobulated margins with the country rocks as observed along Geyikli roadcuts. They are also found in the form of stocks, as evidenced by the hill on which Aladağ village is situated,which is partly composed of such stock. Petrographic analysis reveals euhedral prismatic, pheno- and micro-crystals of clinopyroxene, diopsitic in composition, as the main mafic phase, accompanied by olivine microphenorystals with reaction rims (Figure 5c-d). Similarly, feldspars also indicate that equilibrium is not reached in these magmas, thus when found in the form of phenocrystals, plagioclase crystals are usually mantled by K-feldspar (Figure 5c-d). Biotite, along with feldspars, is a groundmass phase. Leucite phenocrystals are extensively pseudomorph by K-feldspars and enriched with apatite and clinopyroxene inclusion (Figure 5e-g). Apatite is the major accessory mineral in both types of the tephriphonolites and zircon is absent.

In addition to the mafic microgranular enclaves and tephriphonolitic dykes in the pluton, we identified an ellipsoidal block of dark, massive, holocrystalline, granular dioritic rock (~5 x 3 m in size) near Kemallı. Its contact with the country rocks is unclear due to vegetation and debris of its own (Figure 2c-d). A recent study reported the presence of essexite dykes within the pluton, describing them having predominantly pyroxene accompanied by plagioclase, amphibole, K-feldspar with zircon, apatite and monazite with a porphyrtic texture in contact zone (Unluer et al., 2021). According to the glossary of igneous terms, essexite is “a variety of nepheline-bearing monzogabbro or nepheline monzodiorite containing titanian augite, kaersutite and/or biotite with labrodorite, lesser alkali feldspar and and nepheline” (Le Maitre, 2002). The term was first used for basic rocks consisting of augite, hornblende, biotite, plagioclase and orthoclase and nepheline or sodalite (Washington, 1899), indicating that the presence of foids is essential for the nomenclature of these rocks. Despite Ünlüer et al. (2021) identifying the rocks as 'essexites,' their description lacks evidence for nepheline, an essential rock-forming mineral in essexites. Our detailed examination of representative samples clearly demonstrates the presence of interstitial nepheline, together with plagioclase, K-feldspar and prismatic diopside and biotite phenocrystals/micro-crystals (Figure 5h-i). This confirms that these rocks are more accurately classified as nepheline monzogabbro. Furthermore, while sphene and apatite are abundant, we found no evidence of zircon or monazite, which further distinguishes our observations from the previous descriptions.

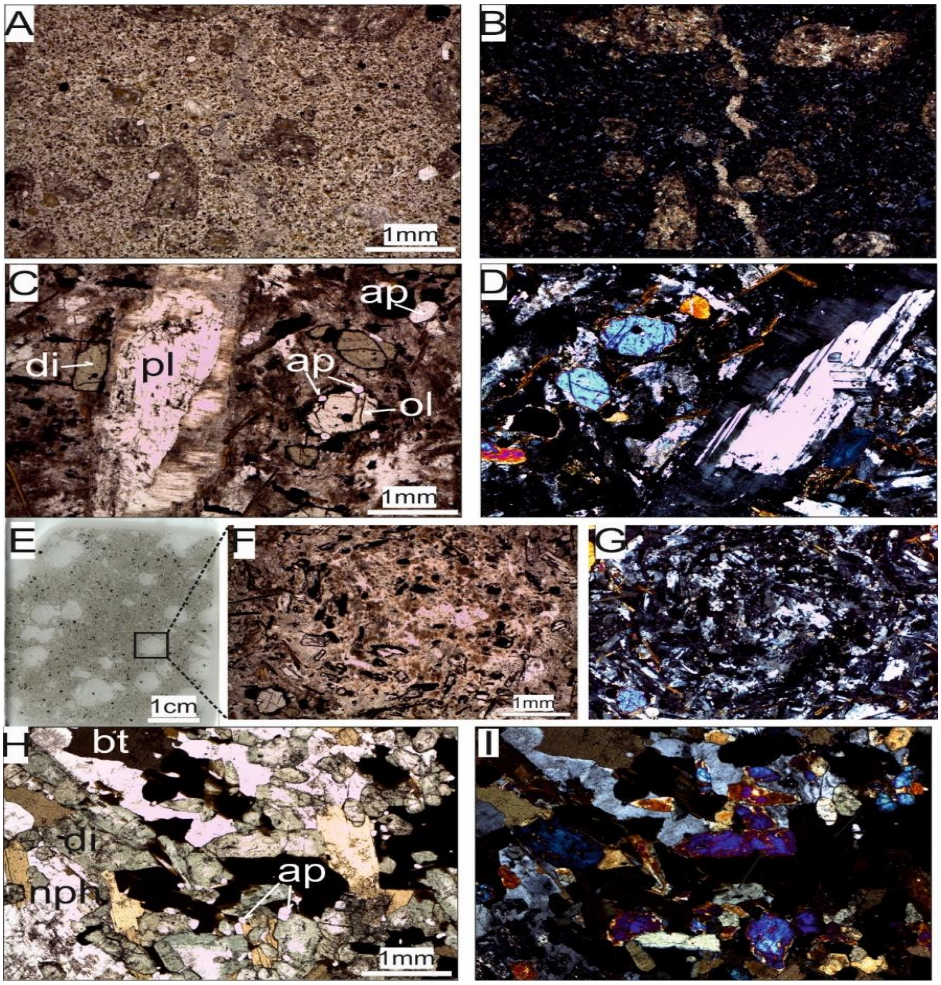

Figure 5. Micro-photographs of the samples representing the mafic dykes and the nepheline monzogabbro block within the Kestanbol pluton, a) plane polarized light view of leucite-aphyric tephriphonolite with hemicrystalline porphyritc texture, biotite and clinopyroxene crystals replaced by secondary minerals due to intensive alteration, b) cross polarized light view of the same area, c) highly porphyritic texture in leucite-phyric tephriphonolite sample with euhedral microphencrystals of diopsite (di) and olivine (ol), and subhedral plagioclase (pl) phenocrystal mantled by K-feldspar, apatite (ap) microcrystals reaching up to 0.2 mm, d) cross polarized light view of the same area, e) scanned thin section showing highly porphyritic texture resulted from the pseudo-leucite phenocrystals, f) pseudo-leucite phenocrystal with apatite and clinopyroxene inclusions, g) cross-polarized view of the pseudo-leucite h) intersertial nepheline (npl), hipidiomorphic biotite, idiomorphic diopsitic clinopyroxene and altered feldspars with abundant apatite microcrystals, i) cross polarized light view of the same area.

Şekil 5. *Kestanbol plütonu içindeki mafik dayklara ve nefelin monzogabro blokuna ait temsilci numunelerin mikro-fotoğrafları, a) hemikristalin porfirik dokulu lösit-afirik teprifonolitte ikincil minerallerce ornatılmış biyotit ve klinoprioksen kristallerinin doğal ışıkta görünümleri, b) aynı alanın polarize ışıkta görünümü, c) ileri derecede porfirik doku sergileyen lösit-firik teprifonolitte öhedral diopsit (di) ve olivin (ol) mikrofenokristalleri, K-feldispat ile çevrelenmiş subhedral plajiyoklas (pl) fenokristali ve 0.2 mm'ye ulaşan büyüklükte apatit (ap) mikro kristalleri, d) aynı alanın polarize ışıkta görünümü, e) lösit-firik tefrifonolite ait taranmış ince kesitte lösit fenokristallerinden kaynaklanan ileri derecede porfirik doku, f) apatit ve klinopiroksen kapantıları içeren psödo-lösit fenokristalinin doğal ışıkta görünümü, g) psödo-lösitin polarize ışıkta görünümü, h) nefelin monzogabro örneğinde intersertal nefelin (npl), hipidiyomorfik biyotit, idiyomorfik diyopsitik klinopiroksen ve altere feldspatlar, bol miktarda apatit mikrokristalleri, i) aynı alanın polarize ışıkta görünümü.*

Volcanics

Miocene volcanism in the region produced lava- and pyroclastic-dominated successions in the region, named as Ayvacık and Balabanlı volcanics. Ayvacık volcanics consist of rhyolitic to dacitic lavas and associated breccias and tuffs, which are widely outcropping out as an envelope to the east and south of the plutonic complex. Silicification and hydrothermal alteration processes extensively affected these lithologies and formed clay enrichments along the faults. These lavas overlie Kestanbol pluton but are also found as dykes intruding the plutonic complex. Andesitic lavas and lahar deposits extending from Ezine to Ayvacık, dominates upper part up the succession. Ayvacık volcanics were identified with the presence of typical rock forming minerals such ascplagioclase, quartz, K-feldspar, biotite, hornblende along with accessory minerals, like sphene, epidote, apatite, and zircons (Karacık, 1995).

The Balabanlı volcanics, located south of the Biga Peninsula and bordered by Tuzla Fault to the north, are dominated by pyroclastic deposits with the limited input of lavas of andesitic, latitic and rhyolitic compositions (Figure 1). Pyroclastic facies include base surges, welded, and non-welded ignimbrites, with volcanic clasts embedded in a pumice-ash matrix. The youngest unit is rhyolitic, forming the Tuzla dome, with abundant quartz, alkali feldspar, biotite, and hornblende. Accessory minerals, such as apatite, rutile, and zircon, occur as inclusions in plagioclase and biotite.

Cover Units

The sedimentary cover units exposed in the area running parallel along the coast. At the base, the cover units are represented by coarse-grained, chaotic deposits that change upward into conglomerates made up of metamorphic and plutonic rock fragments. The accumulation of this clastic package controlled by the adjacent fault blocks (Karacık and Yılmaz, 1998). Above it lies, a fossil-rich, micritic white limestone that date to the Late Miocene-Early Pliocene (Karacık and Yılmaz, 1998).

GEOCHEMICAL AND RADIOGENIC FEATURES OF THE BEACH SANDS AND ROCK UNITS

Bulk rock data indicate that metapelites within the basement rocks have the highest uranium (2.96 ppm) and thorium (12.35 ppm) contents, though they remain within upper crustal values (Yiğitbaş et al., 2014). Measurements of the metamorphic rocks, from outcrops west of Geyikli and south of Tavaklı, confirm that the contribution of these rocks is negligible to total radioactivity (^{238}U: 1-53 Bq kg^{-1}, ^{232}Th: 1-27 Bq kg^{-1}, ^{40}K: 1-50 Bq kg^{-1}; Örgün et al., 2007). In contrast, the Kestanbol pluton, with its monzonitic-quartz monzonitic rocks and their mafic microgranular enclaves with monzodioritic, dioritic compositions, exhibits elevated U (7.3 – 17.4 ppm) and Th (33 – 80 ppm) (Şahin et al., 2012; Öztürk et al., 2020) levels. These concentrations classify the Kestanbol pluton as a uranium-rich variety, as the granites with uranium contents exceeding 12 ppm are typically called as uranium granites (Tassinari, 1992; Peiffert et al., 1994).

More significantly, felsic and mafic dykes within the pluton have even higher concentrations of uranium and thorium with felsic dykes (SiO_2: 60.4 - 77.7 wt.%) containing, 8-29 ppm uranium and 39 – 61 ppm thorium (Şahin et al., 2012). In contrast, tephriphonolitic mafic dykes (SiO_2 < 53 wt.%) with leucite-phyric (U: 22 – 34 ppm, Th: 92 – 114 ppm) and leucite-aphyric (U: 13 – 18 ppm, Th: 50 – 74 ppm) varieties have the highest uranium and thorium concentrations (Akal, 2012).

Published data (Örgün et al., 2007) indicates that the plutonic and likely the hypabyssal rocks of the magmatic association in the region show the highest specific activities of uranium-series (^{238}U: 91-361 Bq kg^{-1}), thorium-series (^{232}Th: 110-341 Bq kg^{-1}) and potassium (^{40}K: 670-1572 Bq kg^{-1}) suggesting a strong association between mineralogic and radionuclide concentrations of these rock.

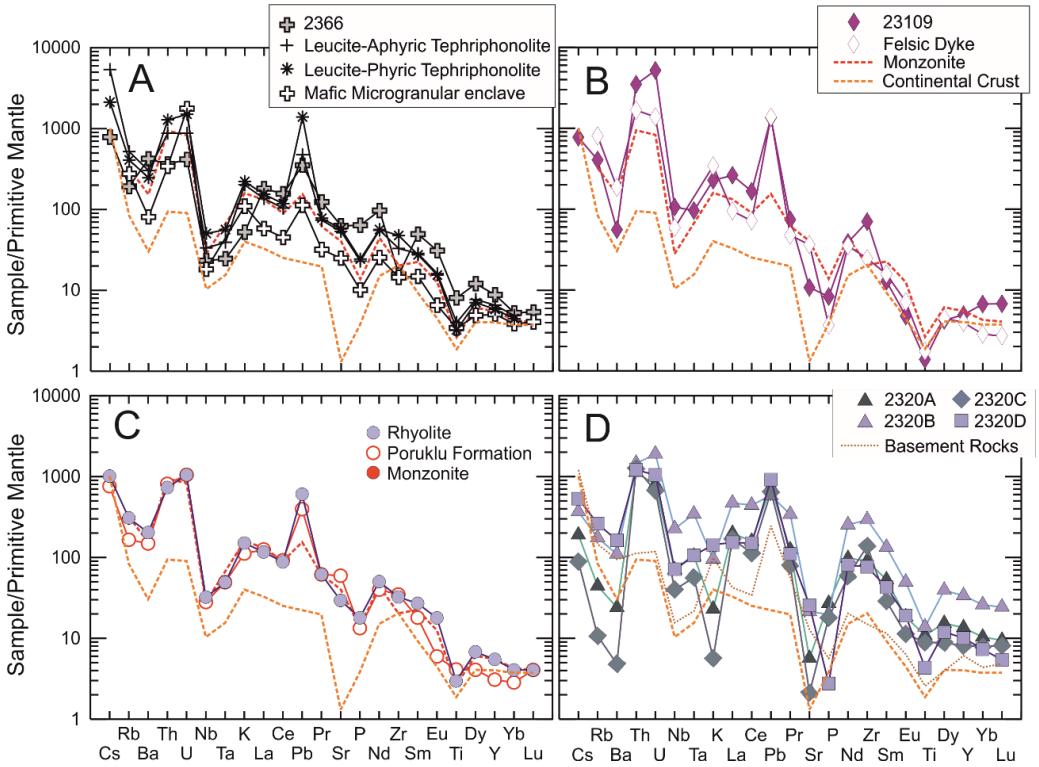

Figure 5. Primitive mantle normalized multi element patterns for the samples a) patterns for nepheline monzogabbro (2366) sample from this study with samples of leucite-aphyric, leucite-phyric tephriphonolites and of mafic microgranular enclave, b) patterns for alkali feldspar pegmatite (23109) with a representative felsic dyke and monzonite sample, c) patterns for representative samples of rhyolitic lava of Ayvacık volcanics, Poruklu formation, monzonite and continental crust, d) patterns for sand fractions of this study. Basement rock is the average of metapelitic rocks of Karadağ Formation (Yiğitbaş et al., 2014), continental crust is from Condie (1993), monzonite, mafic microgranular enclave and felsic dyke are from Şahin et al. (2010), leucite-phyric (LP) and leucite aphyric (LA) tephriphonolites are from Akal (2013), Poruklu Formation and rhyolitic lava are from Öztürk et al. (2020).

Şekil 5. *Örneklerin ilksel mantoya normalize çoklu element desenleri a) nefelin monzogabbro (2366), lösit-afirik, lösit-firik teprifonolit ve mafik mikrogranüler enklav örnekleri, b) radyojenik pegmatit (23109) ile felsik dayk ve monzonitlere ait örnekler, c) Ayvacık volkaniklerinin riyolitik lavları, Poruklu formasyonu, monzonit ve kıtasal kabuğu temsil eden örnekler, d) kum fraksiyonları. Temel kaya Karadağ Formasyonu'nun metapelitik kayaçlarının ortalamasını temsil etmektedir (Yiğitbaş vd, 2014), kıtasal kabuk Condie (1993), monzonit, mafik mikrogranüler anklav ve felsik daykı temsil eden örnekler Şahin vd. (2010), lösit-firik (LP) ve lösit afirik (LA) teprifonolitler Akal (2013), Poruklu Formasyonu ve riyolitik lavlar Öztürk vd.'den (2020) alınmıştır.*

Örgün et al. (2007) also noted that the volcanic rocks exhibit elevated natural radioactivity, largely due to the high specific activity of ^{40}K which can reach up to 1400 Bq kg^{-1} comparable to that of plutonic rocks. However, the specific activities of uranium- series (^{238}U: 40 - 114 Bq kg^{-1}) and thorium-series (^{232}Th: 50 - 168 Bq kg^{-1}) radionuclides in these rocks are lower than in the plutonic rocks, yet remain above Earth's average. Whole rock data show that early rhyolitic, dacitic and trachytic lavas of the Ayvacık volcanics have elevated uranium (7-22 ppm) and thorium (33-66 ppm) contents and exhibits similarities with monzonitic host rocks of the Kestanbol pluton (Figure 6c). The lavas found as flows or clasts within pyroclastic deposits of Balabanlı volcanics exhibit elevated uranium (14 – 18 ppm) and thorium (52 -57 ppm) concentrations in some trachyandesitic lava samples (Aldanmaz et al., 2000; Öztürk et al., 2020).

MATERIALS AND METHODS

Collection and Preparation of the Samples

Representative sand and rock samples were derived from the field for analysis. Sand samples were collected using a Geiger counter from sites with the highest dose rate at Hantepe Beach, Odunluk İskelesi and Akliman. Representative rock samples were derived from the alkali feldspar pegmatite vein, nepheline monzogabbro block and leucite-phyric and leucite-aphyric tephriphonolite for petrographic, gamma spectrometry and bulk geochemical analysis.

As stated by Çetiner et al. (2011), black sand occurrences form lenses with no lateral or vertical continuity. To account for the effect of current action on heavy mineral deposition, samples were taken from the bottom and top of the lenses at and in reverse current direction. The samples were washed in the laboratory to remove organic material such as shell and plant fragments. The ferromagnetic minerals were then removed using a hand magnet, and the samples were then separated into fractions using 250, 180, 125-micron sieves. Finally, a stereomicroscopic examination was conducted to asses grain size distribution across different mineral groups. The 180-250 micron and 125-180 micron sand fractions were re-treated using a Frantz magnetic separator at 0.5 amps current and 20° side inclination, separating a diamagnetic phase (felsic minerals) from a paramagnetic phase (mafic minerals). All sand fractions were examined using stereomicroscopy, X-ray Diffraction (XRD) analysis and bulk geochemical analysis to determine their mineralogical and geochemical compositions. Epoxy embedded polished sections were also prepared for in situ mineral analysis.

The shaking table method was also applied for a single sample derived from Hantepe Beach, without pre-treatment to obtain the heavy minerals, however, the quantity was insufficient for further gamma spectrometry analysis.

Rock samples were crushed in a steel jaw crusher to a grain size of 1-2 mm for gamma spectrometry analysis and powdered using an agate mill for whole rock geochemical analysis.

Gamma Spectrometry

Crushed rock samples and sand fractions were dried and placed in airtight sample containers for activity measurements. The empty containers were weighed five times to record the mean mass, and the samples were weighed again to determine net mass. Samples were stored for at least 21 days to establish radium-radon equilibrium. Measurements were performed using a Canberra GX2020 High Purity Germanium (HPGe) detector in the Research and Development Department of the Proton Accelerator Facility (PHT) at NUKEN, TENMAK with 20% relative efficiency and resolution of 1.1 keV (full width at half

maximum) at 122 keV and 2.0 keV at 1.33 MeV. Prior to commencing the measurements, a background count was conducted over the course of one day. To achieve this, an empty sample container was placed on the gamma detector in order to ensure accuracy in the analysis of the gamma spectrum. Each sample was then similarly positioned on the detector and a one-day count was performed. Following this, a gamma spectrum analysis was conducted for each sample. The resulting gamma spectrum of sample 2320A is provided in Supplementary Data File 1 (Figure 1).

XRD Analysis

The sand fractions were analysed using X-ray diffraction (XRD) at the Central Laboratory of

Konya Technical University. 11 representative samples were ground with tungsten carbide mill to reduce the particle size <10 µm. All samples were analysed using a Europe GNR diffractometer. XRD data were collected using CuKa radiation (40 mA, 40 kV), scanning range of 5-72º 2θ, 0.02º sec/step, 0.250 mm divergence slit. Further details of the XRD analysis with the results are given in the Supplementary Data File 1.

In situ and Bulk Geochemical Analysis

Comprehensive in-situ and whole rock geochemical analysis of sand fractions and rock samples were conducted at the Geochronology and Geochemistry Laboratory, Istanbul University-Cerrahpaşa, Department of Geological Engineering following the measurement and evaluation procedures described by Göçmengil et al. (2021).

The analysis encompassed major oxides, rare earth elements (REE), and trace elements. Major oxide and trace elements, including REEs, were quantified using laser ablation inductively coupled plasma mass spectrometry (LA-ICP-MS). The analysis was performed using a Perkin Elmer NexION 2000 system paired with an ESI NWR-213 laser ablation system. Samples and standard reference materials (SRMs) were ablated with an irradiance of approximately 5 J/cm², a spot diameter of 60 µm, and a laser pulse rate of 10 Hz. The plasma power was set at 1200 watts, with helium as the sample gas (flow rate 0.6 L/min) and argon as the compensation gas (flow rate 0.6 L/min). Each element was analysed over a 30-second period. Calibration was performed after every 15 sample analyses using NIST612 and USGS reference standards BCR-2G and AGV-2G (Jochum et al., 2005). Data analysis was conducted using the ICPMSDataCal software package (Lin et al., 2016). The detailed results of the in-situ analysis of the sand fractions are given in the Supplementary Data File 2.

RESULTS

Sand Fractions

Gamma spectrometry, in-situ and bulk geochemical analysis on sand fractions are presented Table 2, Table 3 and Table 4, respectively.

Overall, a comparison of the total specific activity concentrations on the samples of Hantepe, Odunluk and Akliman beaches, confirm the previous findings with Hantepe exhibiting the highest levels along the coast line (^{238}U-series: 2164.1 Bq/kg, ^{232}Th-series: 2812.7 Bq/kg and ^{40}K: 2775.7 Bq/kg). The sample from Akliman which is far south from Hantepe, has higher total activity (^{238}U-series: 625.7 Bq/kg, ^{232}Th-series: 971.6 Bq/kg and ^{40}K: 1662.9 Bq/kg) than the Odunluk sample (^{238}U series: 771.1 Bg/kg, ^{232}Th-series 855.9 Bq/kg and ^{40}K: 1242.1 Bq/kg) but all within the range of the values observed in the high natural back ground radiation areas of Greece such as Naxos and Mykonos (Papadopoulas et al., 2016).

Table 2. Specific activity concentrations of primordial radionuclides (^{238}U series, ^{232}Th series, and ^{40}K) in the sand fractions with different grain size and mineralogical composition. Total indicates the radioactivity concentration of the bulk sand samples collected from Hantepe, Odunluk and Akliman beaches. The Earth's average values for each radionuclide are provided for comparison.

Tablo 2. *Farklı tane boyu ve mineralojik bileşime sahip kum fraksiyonlarında doğal radyonüklitlerin (^{238}U serisi, ^{232}Th serisi ve ^{40}K) aktivite konsantrasyonları. Toplam değerler, Hantepe, Odunluk ve Akliman plajlarından derlenen kum örneklerinin toplam aktivite konsantrasyonlarını ifade etmektedir. Karşılaştırma için radyonüklidlerin Dünya ortalamaları verilmiştir.*

					Spesific Activity (Bq kg^{-1})					
Sample	Fraction	Location	Grain Size(μ)		^{238}U	SD	^{232}Th	SD	^{40}K	SD
2320A	Mafic	Hantepe	180		267.71	18.77	356.90	28.63	323.08	43.50
2320B	Felsic		180		827.63	73.15	917.66	88.50	883.23	100.78
2320C	Mafic		125		891.05	56.97	1339.25	99.58	397.83	46.02
2320D	Felsic		250		177.68	18.25	198.92	22.91	1171.60	133.34
				Total	2164.1		2812.7		2775.74	
2321A	Mafic	Odunluk	180		268.79	21.95	493.47	44.49	342.89	40.50
2321B	Felsic		180		502.35	51.38	362.44	39.97	899.24	103.10
				Total	771.1		855.9		1242.1	
2336A	Mafic	Akliman	250		63.21	4.73	231.98	19.02	268.03	31.83
2336B	Felsic		250		106.70	10.30	88.13	9.49	575.35	66.80
2336C	Mafic		180		67.46	5.24	302.63	25.47	187.93	23.02
2336D	Felsic		180		326.53	30.77	259.99	26.79	497.15	58.09
2336E	Mafic		125		61.79	4.13	88.91	6.98	134.47	16.72
				Total	625.7		971.6		1662.9	
Earth's Average					33		45		420	

for the coarsest sand fraction (> 250 μm) from Hantepe sample, dominated by felsic minerals (2320D) such as sanidine, albite, anorthose, quartz with minor quantities of clay minerals, revealed by XRD analysis (Supplementary Data File 1), the ^{40}K activity concentration is the highest (1173.3 ± 133.5 Bq/kg) among all other fractions. Although this fraction has low ^{238}U (176.4±18.1 Bq/kg) and ^{232}Th series (197.8±21.9 Bq/kg) activity concentrations, both are higher than Earth's average. It contains 4.3 wt.% K_2O, 21.9 ppm U, 102.9 ppm Th and 576 ppm ∑REE. In contrast, the fraction of 180 μm (2320B), despite having the same minerals based on the microscopic examinations and XRD analysis, exhibit different radionuclide and element concentrations. ^{40}K concentration (883.2 ± 100.8 Bq/kg) is lower, while ^{238}U series (827.6 ± 73.2 Bq/kg) and ^{232}Th series (917.7 ± 88.5 Bq/kg) are significantly higher. Although, its major element composition exhibits slight difference, e.g., with a K_2O content of 2.9 wt.%, its trace element composition is not comparable with other felsic fraction in U (39.8 ppm), Th (123.8 ppm) and in ∑REE which reached up to 1753 ppm as illustrated in primitive mantle normalized multi element variation diagrams (Figure 6a). In-situ analysis on the epoxy embedded mineral grains with examinations under stereomicroscopic confirm the presence of minerals align with the compositions representing uranothorite, thorite and allanite minerals along with abundant zircon and sphene in this fraction (Table 3).

The mafic mineral-dominated fractions (2320A: 180 μm and 2320C: 125 μm) are mineralogically heterogenous, but dominated by hornblende, biotite, olivine, epidote, sphene and zircon. Both fractions show lower ^{40}K

activity concentration (2320A: 323.1 ± 43.5 and 2320C: 397.8 ± 46 Bq/kg) than Earth's average (420 Bq/kg) reflecting the lack of tectosilicates. However, the smaller fraction has much higher ^{232}Th- (1339.3 ± 99.6 Bq/kg) and ^{238}U- series (891.1 ± 56.9 Bq/kg) specific activity concentrations compared to the larger grain size (^{238}U-series: 267.7 ± 18.8 and ^{232}Th-series: 356.9 ± 28.6 Bq/kg). This is evidenced by the slight differences in Th (2320A: 95.8 ppm and 2320C: 106.8 ppm) and ∑REE (2320A: 668 ppm, 2320C:468 ppm) contents of mafic fractions, whereas both have low K_2O (2320A: 0.7 and 2320C: 0.2 wt.%) and uranium (2320A: 16.8 ppm, 2320C: 14.1 ppm). Despite the noise from accidental hydroxide minerals such as magnetite and hematite survived magnetic separation, the peaks correspond to thorite were identified within this fraction along with zircon and ilmenite (Supplementary Data File 1). The finding of thorite group minerals, were also confirmed by in-situ analysis which also revealed the presence of rare grains with compositions consistent with allanite.

Placers from Odunluk and Akliman beaches are also characterized by high activity concentrations. Only two fractions from the Odunluk sample had sufficient quantities for gamma spectrometry analysis. The felsic mineral-dominated fraction (180 µm) consisting of feldspar, quartz and trace amount of zircon (Supplementary Data File 1) has higher specific activity concentrations of ^{238}U series (502.4 ± 51.4 Bq/kg) and ^{40}K (899.2 ± 103.1 Bq/kg), and lower ^{232}Th series (362.4 2 ± 39.9 Bq/kg) compared to the mafic fraction dominated by hornblende, magnetite with trace amount of hematite (^{238}U series: 268.8 ± 21.9 Bq/kg, ^{40}K: 342.9 ± 40.5, ^{232}Th series: 493.5 ± 44.5 Bq/kg).

Notably, mafic mineral dominated fractions from Akliman samples show the lowest ^{238}U-series (2336A: 63.2 ± 4.7 Bq/kg, 2336C: 67.5 ± 5.2 Bq/kg, 2336E: 61.8 ± 4.1 Bq/Kg) and ^{40}K activity concentrations (2336A: 268.0 ± 31.8 Bq/kg, 2336C: 187.9 ± 23.0 Bq/kg, 2336E: 134.5 ± 16.7 Bq/Kg) independent from the grain size. Their ^{232}Th series concentrations vary, with the highest measured in the moderate grain size (302.6 ± 25.5 Bq/Kg) which also consists of allanite (Table 3). Additionally, the smallest grain size (125 µm) has negligible primordial radionuclides concentrations (^{238}U series: 61.8 ± 4.13 Bq/kg, ^{232}Th series: 88.9 ± 6.9 Bq/kg, ^{40}K: 134.5 ± 16.7 Bq/kg). In contrast, the felsic fractions from Akliman have the highest ^{40}K specific activity (2336B: 575.4 ± 66.8 Bq/kg and 2336D: 497.2 ± 58.1 Bq/kg). The smaller grain size (180 µm), has higher ^{238}U- (326.5 ± 30.8 Bq/kg) and ^{232}Th-series (259.9 ± 26.8 Bq/kg) than the larger fraction (250 µm, ^{238}U: 106.7 ± 10.3 Bq/kg, ^{232}Th-series: 88.1 ± 9.5 Bq/kg).

Rock Samples

Gamma spectrometry analysis was conducted on samples representing the alkali feldspar pegmatite vein (Pgm: 23109), the nepheline monzogabbro block (Nmg: 2366) and the leucite-phyric (LfPh: 2373) and leucite-aphyric tephriphonolites (LaPh: 23131) (Table 4). The pegmatitic rock sample reveals the most elevated specific activity concentrations of primordial radionuclides (^{238}U series: 1164.3 ± 13.2 Bq/kg, ^{232}Th series 709.6 ± 17.4 Bq/kg, ^{40}K: 1783.5 ± 56 Bq/kg) among all previously reported values for rocks (Örgün et al, 2007) in the vicinity of the Hantepe beach (Figure 6 b). It has the most elevated Th (297.4 ppm) and U (108.9 ppm) contents with moderate ∑REE (572 ppm).

Leucite-phyric tephriphonolite sample also exhibits elevated radionuclides concentrations, with specific activities of 524.7 ± 6.3 Bq/kg for ^{238}U series, 309.4 ± 7.8 Bq/kg for ^{232}Th series and 1760.5 ± 55.4 Bq/kg for ^{40}K. In contrast, the cogenetic leucite-aphyric tephriphonolite displays significantly lower specific activity concentrations (^{238}U series: 195.6 ± 3.1 Bq/kg, ^{232}Th series: 45.9 ± 1.5 Bq/kg and ^{40}K: 77.1 ±4.3 Bq/kg).

Table 3. Representative in-situ analysis on epoxy embedded mineral grains of felsic (2320B, 180µ; 2336D, 180µ) and mafic (2320A, 180µ; 2320C,125 µ; 2336C, 180µ) mineral dominated fractions of the sand samples from Hantepe and Akliman beaches (Spn: sphene, Thr: thorite, Zrn: zircon, U-Thr: uranothorite, Aln: allanite).

Tablo 3. *Hantepe ve Akliman plajlarından derlenen kum örneklerinde felsik (2320B, 180µ; 2336D, 180µ) ve mafik (2320A, 180µ; 2320C,125 µ; 2336C, 180µ) minerallerce zengin fraksiyonlarda noktasal mineral analizlerleri (Spn: sfen, Thr: torit, Zrn: zirkon, U-Thr: urnotorit, Aln: allanit).*

Sample	2320A	2320 B			2320 C			2336C	2336D	
Mineral	Spn	Thr	Zrn	Zrn	U-Thr	Zrn	Zrn	Aln	Spn	Zrn
wt.%										
SiO_2	28.86	14.25	29.79	29.78	15.08	30.88	30.08	27.42	29.21	30.06
TiO_2	35.64	0.13	0.00	0.00	0.05	0.01	0.00	38.80	38.56	0.00
Al_2O_3	1.17	0.00	0.00	0.00	0.00	0.00	0.00	1.44	1.08	0.28
FeO	2.34	0.00	0.00	0.00	0.01	0.28	0.11	2.56	1.96	0.00
MnO	0.11	0.00	0.00	0.00	0.00	0.00	0.00	0.12	0.12	0.00
MgO	0.04	0.00	0.00	0.00	0.00	0.00	0.00	0.04	0.03	0.00
CaO	25.61	0.00	0.00	0.02	0.00	0.00	0.00	23.25	25.15	0.00
Na_2O	0.04	0.00	0.00	0.00	0.00	0.00	0.00	0.03	0.03	0.02
K_2O	0.01	0.00	0.00	0.00	0.00	0.00	0.00	0.00	0.00	0.20
P_2O_5	1.91	0.05	0.03	0.03	0.01	0.05	0.02	0.05	0.08	0.03
ppm										
Y	2612.40	564.62	611.68	2008.51	324.10	660.01	603.84	6217.45	753.20	1350.80
Hf	126.96	1.97	6910.54	8385.60	1.27	10421.47	10289.86	66.20	57.27	12065.57
Zr	655.52	227.93	501053.40	495387.70	109.64	486032.10	493823.40	917.16	750.11	529898.50
Th	358.13	553958.30	273.26	1359.15	458302.60	631.53	616.68	912.94	531.63	915.65
U	287.10	28475.60	265.21	911.31	141218.10	663.49	633.51	134.00	687.91	674.12
∑ *REE*	21174	2180	420	1149	869	514	473	35567	22909	869

This finding also has supported by the bulk geochemical composition of these two types of hypabyssal rocks in the Kestanbol pluton. According to the available data from Akal (2012) the leucite-phyric variety having higher U (av. 30 ppm), Th (av.105 ppm) and ∑REE (462 ppm) contents than the leucite-aphyric one (av. U: 15 ppm, av. Th: 61 ppm, av. ∑REE: 397 ppm).

On contrary to the claims of previous studies, gamma spectrometry analysis show that nepheline monzogabbro sample has the lowest ^{238}U (103.7 ± 1.6 Bq/kg) and ^{232}Th series (81.3 ± 2.3 Bq/kg) activities, but it shows a comparatively high ^{40}K activity (999.9 ± 32.3 Bq/kg) with a high ∑REE (634.9) content. However, it consists of very low U (8.7 ppm) and Th (31.1 ppm).

Table 4. Bulk analysis of sand fractions and rock samples. Sand fractions represent Hantepe beach sample (Nmg: nepheline monzogabbro, Pgm: radiogenic pegmatite, Mnz: monzonite Mme: mafic microgranular enclave, FD: felsic dyke, LP: leucite-phyric tephriphonolite, LA: leucite-aphyric tephriphonolite, PH: Poruklu hypabyssal rocks, Rhy: rhyolitic lavas, [1]: Şahin et al., 2010; [2]: Akal, 2013; [3]: Öztürk et al., 2020).

Tablo 4. *Kum fraksiyonları ve kayaçların tüm kayaç jeokimya analizleri. Kum fraksiyonları Hantepe plajı örneğine aittir (Nmg: Nefelin monzogabro, Pgm: radyojenik pegmatit, Mnz: monzonit, Mme: mafik mikrogranüler anklav, FD: felsik dayk, LP: lösit-firik tefrifonolit, LA: lösit-afirik tefrifonolit, PH: Poruklu hipabisal kayaları, Rhy: riyolitik lavlar, [1]: Şahin vd.,2010; [2]: Akal (2013), [3] Öztürk vd., 2020).*

	Sand Fractions				Rock Samples								
Sample No	2320A	2320B	2320C	2320D	2366	23109	4	15--1	52--2	2254/12	2254/6	13–31	13-46B
Type	Mafic	Felsic	Mafic	Felsic	Nmg	Pgm	Mnz	Mme	FD	LP	LA	PH	Rhy
Grain Size	180	180	125	250									
Reference							[1]	[1]	[1]	[2]	[2]	[3]	[3]
SiO_2	15.14	75.42	8.53	77.33	44.00	63.11	63.18	53.7	60.4	52.65	50.97	74.84	58.89
TiO_2	2.36	2.99	1.93	0.94	1.75	0.30	0.57	0.74	0.38	0.7	0.87	0.89	0.64
Al_2O_3	2.70	8.45	1.07	9.40	10.86	15.06	15.63	14.5	17.34	18.43	15.69	13.15	16.1
FeO	73.34	1.22	84.79	1.00	13.09	1.92	4.00	6.53	1.79	5.27	6.03	1.15	4.52
MnO	0.29	0.03	0.27	0.02	0.21	0.06	0.08	0.2	0.07	0.13	0.16	0.01	0.1
MgO	0.00	0.00	0.00	0.00	8.34	0.31	2.12	7.57	0.35	2.87	3.57	0.21	2.79
CaO	2.61	3.91	1.57	2.19	13.98	1.68	4.14	7.48	2.06	5.7	6.16	0.21	3.3
Na_2O	0.75	1.83	0.25	1.98	2.72	6.42	3.56	3.23	3.07	4.08	3.86	0.11	3.34
K_2O	0.69	2.87	0.17	4.32	1.58	6.84	4.79	3.31	10.28	6.68	6.07	3.36	4.54
P_2O_5	0.59	0.43	0.39	0.06	1.39	0.18	0.3	0.22	0.08	0.53	0.5	0.29	0.39
LOI	1.08	2.31	0.58	2.08	1.01	3.82	0.7	1.5	3.7	1.8	4.9	5.2	4.4
Total	99.55	99.47	99.55	99.31	98.94	99.70	99.51	99.9	96.02	99.44	99.46	99.54	99.52
Sc	16.6	14.5	15.9	16.8	47.3	14.0				12.0	17.0	18.0	11.0
V	1717.6	108.4	2004.7	65.0	311.8	62.4	95.0	149.0	42.0	135.0	161.0	132.0	127.0
Cr	1802.1	58.7	2292.9	42.8	215.6	50.2							
Co	59.4	2.7	62.3	2.1	50.4	3.8	13.0	29.0	1.9	27.6	30.0	11.0	25.0
Ni	58.2	14.7	52.2	8.3	46.8	4.5				11.6	25.4	1.0	16.0
Ga	36.0	34.1	32.9	17.4	24.0	33.8	19.0	17.0	16.0	19.0	17.3	16.0	22.0
Ge	5.9	6.5	4.7	1.8	3.4	1.2							
Rb	28.2	110.9	6.8	166.1	122.1	257.6	204.0	175.0	510.0	260.2	330.9	105.0	195.0
Sr	119.4	450.9	44.5	539.8	1324.8	226.8	850.0	527.0	767.0	1216.6	1129.2	1251.0	619.0
Y	61.5	153.0	36.8	45.9	40.1	22.5	25.0	23.0	18.0	26.5	29.9	14.0	25.0
Zr	1015.6	3266.3	1552.5	855.3	175.3	783.6	228.0	162.0	274.0	532.6	368.7	389.0	363.0
Nb	49.9	161.3	28.5	50.9	16.6	75.6	20.0	13.0	42.0	36.0	23.9	20.0	23.0
Cs	1.5	2.9	0.7	4.2	6.2	6.1				16.8	42.5	6.0	8.0
Ba	168.2	766.4	33.6	1133.9	2956.7	388.0	1072.0	565.0	1298.0	1722.0	2121.0	1040.0	1420.0
La	136.2	323.2	116.1	105.5	124.4	179.8	91.0	39.8	65.0	106.2	93.6	86.0	80.0
Ce	282.0	787.1	199.5	266.1	277.9	294.3	159.0	80.0	127.0	209.3	184.5	164.0	156.0
Pr	34.4	94.3	21.9	30.4	34.2	20.4	17.0	8.8	13.1	21.5	20.3	17.0	17.0
Nd	131.8	343.3	79.0	109.4	131.3	52.5	60.0	34.4	47.6	76.6	75.1	54.0	68.0
Sm	23.5	59.2	12.8	19.0	22.0	5.7	10.0	6.6	7.0	12.2	12.7	8.0	12.0
Eu	3.1	8.3	1.9	3.2	5.2	0.8	2.1	1.1	1.2	2.6	2.7	1.0	3.0
Gd	29.5	66.4	16.4	22.4	20.0	7.1	6.5	4.6	4.7	8.5	9.1	5.0	9.0
Tb	2.5	6.3	1.4	1.9	1.9	0.6	0.9	0.7	0.8	1.1	1.2	1.0	1.0
Dy	11.3	28.9	6.5	8.8	8.9	3.1	4.5	3.6	3.3	5.2	5.7	3.0	5.0
Ho	2.0	5.0	1.2	1.6	1.6	0.7	0.7	0.7	0.5	0.8	1.0	1.0	1.0
Er	5.5	14.0	3.3	3.6	3.9	2.3	2.1	2.1	1.4	2.3	2.5	1.0	2.0
Tm	0.8	2.0	0.5	0.5	0.4	0.4	0.3	0.3	0.2	0.3	0.4	0.2	0.3
Yb	5.1	12.8	3.9	3.6	2.6	3.3	2.1	1.9	1.4	2.2	2.4	1.4	2.0
Lu	0.7	1.8	0.6	0.4	0.4	0.5	0.3	0.3	0.2			0.3	0.3
Hf	23.6	64.7	34.4	15.6	6.1	19.1				11.9	8.7	9.0	9.0
Ta	4.2	14.0	2.3	4.3	1.0	3.9				2.3	1.6	2.0	2.0
Pb	52.7	41.4	45.8	65.1	25.0	96.0	11.0	8.0	98.0	98.7	33.8	28.0	43.0
Th	95.8	123.8	106.8	103.0	31.1	297.4	80.0	29.0	142.0	109.0	74.4	69.0	62.0
U	16.8	39.8	14.1	22.0	8.7	108.8	17.4	37.0	29.0	31.6	18.4	22.0	22.0
Zn	406.5	45.0	373.5	28.5	110.8	35.5							

Table 5. Specific activity concentrations of primordial radionuclides (^{238}U series, ^{232}Th series and ^{40}K) in rock samples collected from Kestanbol pluton (Nmg: nepheline monzogabbro, LP: leucite-phyric tephriphonolite, Pgm: alkali feldspar pegmatite, LA: leucite-aphyric tephriphonolite).

Tablo 5. *Kestanbol plütonuna ait kayaç örneklerinde doğal radyonüklitlerin (^{238}U serisi, ^{232}Th serisi ve ^{40}K) spesifik aktivite konsantrasyonları (Nmg: nefelin monzogabro, LP: lösit-firik tefrifonolit, Pgm: Pegmatit, LA: lösit-afirik tefrifonolit).*

		Spesific Activity (Bq kg^{-1})					
Sample	Rock Type	^{238}U	SD	^{232}Th	SD	^{40}K	SD
2366	Nmg	103.7	1.6	81.3	2.3	999.9	32.3
2373	LP	524.7	6.3	309.4	7.8	1760.5	55.368
23109	Pgm	1164.3	13.2	709.6	17.4	1783.5	56.0
23131	LA	195.6	3.1	45.9	1.5	77.1	4.3
Earth's Average		33		45		420	

DISCUSSION

Radiogenic beach sands are typically derived from U- and Th-enriched felsic igneous rocks as observed in Mykonos, Greece (Papadopoulas et al., 2016). It should be noted, however, some beaches might also derive from both magmatic and metamorphic sources. As observed on Naxos Island, a potential site for REE exploitation, and Touzla, Thessaloniki where sands originate from Mesozoic and Paleozoic high-grade metamorphic units of the Aixos of the Hellenides (Filippidis et al., 1997; Papadopoulas, 2018). As the basement rocks in the region do not show significant imprints for radionuclide enrichments, we only focus on the magmatic complex.

The distribution of total radioactivity and the relative contribution of each radionuclide varies significantly along the coastline between Geyikli and Akliman. To better understand this, we have visualized the data published by Örgün et al., (2007) as pie charts on the geologic map (Figure 1). In contrast to the other beaches, Hantepe beach is located at the seaward end of the E-W trending drainage system which developed primarily on metamorphic and ophiolitic basement units, rather than magmatic rocks (Figure 1). Interestingly, samples from Hantepe exhibit the highest specific activities of ^{238}U (1885.2 ± 4.7 Bq/Kg) and ^{232}Th (4360.3 ± 4.6 Bq/Kg) series with moderate ^{40}K (687.1 ± 6.1 Bq/Kg). In contrast, southern beaches, probably composed of materials predominantly derived from the Kestanbol pluton, have higher ^{40}K concentrations (858.2 ± 2.8 – 1389.2 ± 5.2 Bq/Kg) but lower activities in ^{238}U (89.1 ± 1.4 – 205.6 ± 1.3 Bq/Kg) and ^{232}Th (115.5 ± 0.9 - 320.9 ± 1.5 Bq/Kg) series (Örgün et al., 2007).

The heterogeneous mineralogical composition across the pluton or uneven distribution of the specific lithologies hosting radiogenic minerals is a plausible explanation for the high radioactivity at Hantepe beach. A recent study attributed higher dose rates in the northern part of the pluton to thorite and monazite in alkali potassic rocks of the Kestanbol pluton (Döner et al., 2022). If the so-called potassic rocks are indeed the equivalent to the tephriphonolite dykes and stocks of the Kestanbol pluton, as suggested, they cannot be considered as sources of zircon or thorite since they contain mainly apatite. Importantly, leucite-aphyric dykes have the lowest specific activities of ^{238}U- and ^{232}Th- series with ^{40}K and moderate radioelement concentrations. Another study evaluating the radioactive beach sands for their REE potential, suggests that Geyikli placers

are enriched by monazite, apatite and zircon, and that manzogabbro dykes can be considered as the source of the radiogenic minerals (Unluer et al., 2021). However, as shown by gamma spectrometry and bulk chemical analysis with mineralogical investigations, similar to leucite-aphyric dykes, nepheline monzogabbro has low specific activities of ^{238}U- and ^{232}Th- series as well as low radioelement contents, but the highest ∑REE. It is also rich in apatite and sphene but poor in zircon and monazite. In our opinion, their results are only conjectures based on unjustified assumptions. Our analyses also underline that a positive correlation between REE and U, and Th is not always present.

The first study investigating the geological aspects of the high natural background radiation in the region documented the presence of accessory minerals such as sphene, zircon, allanite, apatite, epidote, thorite, uranothorite dispersed in the plutonic rocks, in the range of % 0.1–4.5 (Andaç, 1971, 1973). The presence of uranothorite in the monzonitic rocks was later confirmed by a recent study which provides electron probe micro-analysis (Angı et al., 2017). Contrary to previous investigations supporting the presence of monazite and zircon in beach sands, Andaç (1971) highlighted thorite and uranothorite as the primary radiogenic minerals, found as inclusions in hornblende within the aplitic veins cutting through monzonitic country rocks. Our analysis aligns with this, showing that the tectosilicate-dominated sand fractions and alkali-feldspar pegmatite vein have the highest concentrations of primordial radionuclides and radioelements, which are mainly stored within thorite group minerals found as discrete grains and inclusions. Allanite may be considered a potential radiogenic phase in the beach sands. However, based on the available evidence and observations, it is unclear whether it is concentrated within a specific lithology, such as uranothorite.

All the felsic sand fractions with rock samples, except leucite-aphyric potassic dykes, exhibit elevated ^{40}K concentrations (ranging from 497 to 1784 Bq/kg). Given that K-feldspar is not a main rock forming mineral in the nepheline monzogabbro and leucite-phyric tephriphonolite, other K-bearing minerals, such as foids and biotite, are likely to contribute to the high ^{40}K activity. Rock forming minerals, as well as accessory minerals of the magmatic complex, should also be considered as sources to the radionuclides. It is important to highlight that, all the members of the Miocene Ezine-Ayvacık magmatic system including the volcanic rocks display radionuclide enrichments to different extents, suggesting that the primary magmas were enriched in radionuclides and radioelements (Örgün et al., 2007). This probably resulted in the enrichment of radionuclides in rock forming minerals and groundmass in lavas and pyroclastic rocks. This is evidenced by the fact that the sand sample from Akliman beach, which consists of materials mainly derived from Balabanlı volcanics, also has elevated total radioactivity (Table 2).

An elegant explanation for the high natural background radiation at Hantepe beach lies in its geomorphological and geographical characteristics. It has the largest wet zone among compared to other beaches with a heterogeneous radiation distribution that varies spot by spot and decreases landward (Cetiner, et al., 2011). As part of the natural radiation treatment studies, it was monitored that sand removal significantly reduced the radiation at the beach (Cetiner, et al., 2012). Thus, we conclude that longshore currents, wave action, and more importantly long-lasting transportation from the source are parameters as important as the source rock mineralogy, for the accumulation of abrasion resistant minerals at Hantepe beach in higher concentrations.

CONCLUSION

The present study offers a framework for the source rock characteristics of the radiogenic beach sands. By employing gamma spectrometry analysis in conjuction with geochemical and mineralogical analysis, and by working on the sand fractions, instead of bulk sand samples, this study has revealed the presence of thorite group minerals in the beach sands.

Alkali feldspar pegmatitic veins are the most radiogenic lithologies and have the most elevated uranium and thorium contents within the Ezine-Ayvacık magmatic complex, given that they consist of discrete grains or inclusions of thorite group minerals.

Other rock-forming and accessory minerals, such as zircon, sphene, allanite, apatite have the potential to contribute to high natural background radiation, depending on their host

rocks. This is currently being investigated. The source rock for radiogenic beach sands can be challenging to identify when based on solely whole-rock geochemistry. A more detailed mineralogical approach is essential.

ACKNOWLEDGEMENT

This work resulted from discussions held during the initial field trips to the area , between the team of a scientific project investigating the factors controlling the U-Th enrichments in the Miocene Ezine-Ayvacık magmatic complex (TÜBİTAK-ÇAYDAG, Project No: 122Y164) Bulk analyses of the nepheline gabbro and feldspar pegmatites were conducted under this project. We thank the bachelor students Ayşe Güven, Bilal Kaya, and Cem Gülseven of İstanbul Technical University Geological Engineering Department for their assistance in the separation of sand fractions. We are grateful to Editor E. Varol Muratçay for the editorial work and to two anonymous reviewers for their constructive comments, which improved the early version of the manuscript.

REFERENCES

Akal, C. 2013. Coeval Shoshonitic-ultrapotassic dyke emplacements within the Kestanbol pluton, Ezine–Biga peninsula (NW Anatolia). Turkish Journal of Earth Sciences, 22(2), 220-238. DOI: 10.3906/yer-1202-1

Aldanmaz, E. R. C. A. N., Pearce, J. A., Thirlwall, M. F., Mitchell, J. G. 2000. Petrogenetic evolution of late Cenozoic, post-collision volcanism in western Anatolia, Turkey. Journal of Volcanology

and Geothermal Research, 102(1-2), 67-95. DOI: 10.1016/S0377-0273(00)00182-7

Altunkaynak, Ş., Dilek, Y., Genç, C.Ş., Sunal, G., Gertisser, R., Furnes, H., Foland, K.A.,Yang, J., 2012. Spatial, temporal and geochemical evolution of Oligo-Miocene granitoid magmatism in western Anatolia, Turkey. Gondwana Res. 21, 961–986. DOI: 10.1016/j.gr.2011.10.010

Andaç, M. 1971. Biga yarımadasında tarihi truva harabelerinin güneyindeki radyoaktf sahil kumlarının mineralojisi ve bunların ana kayaçlarının petrolojisi. Bulletin of the Mineral Research and Exploration, 76(76), 75-79.

Andaç, M. 1973. Biga Yarimadasinda Ezine Siyenit Masifi ile Civarindaki Kayaçlarin Petrografisi Ve Bu Kayaçlardan Meydana Gelen Radyoaktif Sahil Plaser Maden Yataginin Etüdü. Istanbul Teknik Üniversitesi, Doçentlik Tezi, 97s, Istanbul.

Aygül, M., Topuz, G., Okay, A., Satir, M., Meyer, H. P. 2012. The kemer metamorphic complex (NW Turkey): a subducted continental margin of the Sakarya zone. Turkish Journal of Earth Sciences, 21(1), 19-35. DOI: 10.3906/yer-1006-14

Aytekin, H., Tufan, M. Ç., Küçük, C. 2015. Natural radioactivity measurements and dose assessments in sand samples collected from Zonguldak beaches in Turkey. Journal of Radioanalytical and Nuclear Chemistry, 303, 2227-2232. DOI: 10.1007/s10967-014-3819-1

Aysal, N., 2015. Mineral chemistry, crystallization conditions and geodynamic implications of the Oligo-Miocene granitoids in the Biga Peninsula, Northwest Turkey. J. Asian Earth Sci. 105, 68–84. DOI: 10.1016/j.jseaes.2015.03.026

Beccaletto, L., Jenny, C. 2004. Geology and correlation of the Ezine Zone: a Rhodope fragment in NW Turkey?. Turkish Journal of Earth Sciences, 13(2), 145-176.

Black, K.N., Catlos, E.J., Oyman, T., Demirbilek, D., 2013. Timing Aegean extension: evidence from in situ U-Pb geochronology and cathodoluminescence imaging of granitoids from NW Turkey. Lithos 181, 92–108. DOI: 10.1016/j.lithos.2013.09.001

Chandrasekharam, D., Baba, A. 2021. High heat generating granites of Kestanbol: future enhanced geothermal system (EGS) province in western Anatolia. Turkish Journal of Earth Sciences, 30(9), 1032-1044. DOI: 10.3906/yer-2106-16

Cetiner, M. A., Gündüz, H., Ilgar, A. 2011. High background radiation areas at Çanakkale in Turkey. Radiation Physics and Chemistry, 80(6), 704-709. DOI: 10.1016/j.radphyschem.2011.02.024

Cetiner, M. A., Gunduz, H., Tukenmez, I. 2012. Natural radiation monitoring and control treatment in the Hantepe beach. Radiation protection dosimetry, 152(4), 429-433. DOI: 10.1093/rpd/ncs050

Döner, Z., Ünlüer, A.T., Özdamar, Ş., Sarıkaya, O., Kaya, M., Kocatürk, H., Kumral, M., Esenli, R.F. 2022. REE-Th-U Enrichments in alkali-potassic rocks in Kestanbol Granitoid Complex (Ezine-Çanakkale, Turkey): Revealing the factors that cause mineralizations. 9th Geochemistry Symposium, 17-22 October, Aydın, 196-203.

Duru M., Pehlivan Ş., Aral İ. O., Şentürk Y., Yavaş, F., Kar H., 2012. Biga Yarımadasının Tersiyer Öncesi Jeolojisi, Maden Tetkik ve Arama Genel Müdürlüğü Yayınları, Özel Yayınlar Serisi, No 28, 326s.

Filippidis, A., Misaelides, P., Clouvas, A., Godelitsas, A., Barbayiannis, N., Anousis, I. 1997. Mineral, chemical and radiological investigation of a black sand at Touzla Cape, near Thessaloniki, Greece. Environmental Geochemistry and Health, 19, 83-88. DOI: 10.1023/A:1018498404922

Göçmengil, G., Tükel, F. Ş., Uzun, F., Guıllong, M., Yılmaz, İ., Aysal, N., Hanilçi, N. 2022. Accurate whole-rock geochemistry analysis by combined ICP-OES and LA-ICP-MS instruments. Bulletin of the Mineral Research and Exploration, 168, 157-165. DOI: 10.19111/bulletinofmre.947703

Hou, B., Keeling, J., Van Gosen, B. S. 2017. Geological and exploration models of beach placer deposits, integrated from case-studies of Southern Australia. Ore Geology Reviews, 80, 437-459. DOI: 10.1016/j.oregeorev.2016.07.016

Karacık, Z., 1995. Relationship Between Young Volcanism and Plutonism in Ezine-

Ayvacık (Çanakkale) Region. İstanbul Technical University, PhD Thesis, İstanbul

Karacık, Z., Yılmaz, Y. 1998. Geology of the ignimbrites and the associated volcano–plutonic complex of the Ezine area, northwestern Anatolia. Journal of Volcanology and Geothermal Research, 85(1-4), 251-264. DOI: 10.1016/S0377-0273(98)00058-4

Karadeniz, Ö., Akal, C. 2014. Radiological mapping in the granodiorite area of Bergama (Pergamon)-Kozak, Turkey. Journal of Radioanalytical and Nuclear Chemistry, 302, 361-373. DOI: 10.1007/s10967-014-3216-9

Kucukomeroglu, B., Karadeniz, A., Damla, N., Yesilkanat, C. M., Çevik, U. 2016. Radiological maps in beach sands along some coastal regions of Turkey. Marine pollution bulletin, 112(1-2), 255-264. DOI: 10.1016/j.marpolbul.2016.08.007

Le Maitre, R. W., Streckeisen, A., Zanettin, B., Le Bas, M. J., Bonin, B., Bateman, P., ... Woolley, A. R. 2002. Igneous rocks. A Classification and Glossary of Terms: Recommendations of the International Union of Geological Sciences Subcommission on the Systematics of Igneous Rocks, Cambridge University Press, Cambridge, 236p.

Mohanty, A. K., Sengupta, D., Das, S. K., Vijayan, V., Saha, S. K. 2004. Natural radioactivity in the newly discovered high background radiation area on the eastern coast of Orissa, India. Radiation measurements, 38(2), 153-165. DOI: 10.1016/j.radmeas.2003.08.003

Okay, A. I., Siyako, M., Bürkan, K. A. 1991. Geology and tectonic evolution of the Biga Peninsula, northwest Turkey. Bulletin of the Technical University of Istanbul, 44(1-2), 191-256.

Okay, A. I., Satır, M. 2000. Upper Cretaceous eclogite-facies metamorphic rocks from the Biga Peninsula, Northwest Turkey. Turkish Journal of Earth Sciences, 9(2), 47-56.

Okay, A. I., Göncüoğlu, M. C. 2004. The Karakaya Complex: a review of data and concepts. Turkish Journal of Earth Sciences, 13(2), 75-95.

Örgün, Y., Altınsoy, N., Şahin, S. Y., Güngör, Y., Gültekin, A. H., Karahan, G., Karacık, Z. 2007. Natural and anthropogenic radionuclides in rocks and beach sands from Ezine region (Canakkale), Western Anatolia, Turkey. Applied Radiation and Isotopes, 65(6), 739-747. DOI: 10.1016/j.apradiso.2006.06.011

Özden, S., Aközcan, S. 2021. Natural radioactivity measurements and evaluation of radiological hazards in sediment of Aliağa Bay, İzmir (Turkey). Arabian Journal of Geosciences, 14, 1-14. DOI: 10.1007/s12517-020-06446-9

Öztürk, Y. Y., Akal, C., Gerdes, A. 2020. U–Pb ages and Hf isotopic compositions of zircon from the Early Miocene Kestanbol Magmatic Complex in NW Anatolia (Turkey): Implications for crustal contribution in the post-collisional magmatism. Journal of Asian Earth Sciences, 192, 104262. DOI: 10.1016/j.jseaes.2020.104262

Papadopoulos, A., Christofides, G., Koroneos, A., Stoulos, S. 2014. Natural radioactivity distribution and gamma radiation exposure of beach sands from Sithonia Peninsula. Open Geosciences, 6(2), 229-242. DOI: 10.2478/s13533-012-0157-0

Papadopoulos, A., Koroneos, A., Christofides, G., Stoulos, S. 2015. Natural radioactivity distribution and gammaradiation exposure of beach sands close to Kavala pluton,

Greece. Open Geosciences, 7(1), 20150043. DOI: 10.1515/geo-2015-0043

Papadopoulos, A., Koroneos, A., Christofides, G., Papadopoulou, L., Tzifas, I., Stoulos, S. 2016. Assessment of gamma radiation exposure of beach sands in highly touristic areas associated with plutonic rocks of the Atticocycladic zone (Greece). Journal of environmental radioactivity, 162, 235-243. DOI: 10.1016/j.jenvrad.2016.05.035

Papadopoulos, A., Altunkaynak, Ş., Koroneos, A., Ünal, A.,& Kamaci, Ö. 2017. Geochemistry of uranium and thorium and natural radioactivity levels of the western Anatolian plutons, Turkey. Mineralogy and Petrology, 111, 677-691. DOI: 10.1007/s00710-017-0492-4

Papadopoulos, A. 2018. Geochemistry and REE content of beach sands along the Atticocycladic coastal zone, Greece. Geosciences Journal, 22, 955-973. DOI: 10.1007/s12303-018-0004-5

Peiffert, C., Cuney, M., Nguyen-Trung, C. 1994. Uranium in granitic magmas: Part 1. Experimental determination of uranium solubility and fluid-melt partition coefficients in the uranium oxide-haplogranite-H_2O-Na_2CO_3 system at 720–770° C, 2 kbar. Geochimica et cosmochimica acta, 58(11), 2495-2507. DOI: /10.1016/0016-7037(94)90026-4

Salters, V. J., Stracke, A. 2004. Composition of the depleted mantle. Geochemistry, Geophysics, Geosystems, 5(5). DOI: i:10.1029/2003GC000597

Şahin, S. Y., Örgün, Y., Güngör, Y., Göker, A., Gültekin, A. H., Karacık, Z. 2010. Mineral and whole-rock geochemistry of the Kestanbol Granitoid (Ezine-Çanakkale) and its mafic microgranular enclaves in northwestern Anatolia: evidence of felsic and mafic magma interaction. Turkish Journal of Earth Sciences, 19(1), 101-122. DOI: 10.3906/yer-0809-3

Tassinari, C. C. G. 1992. Uranium in granitoids: recognition criteria of uranium provinces in Brazil. New developments in uranium exploration, resources, production and demand. Proceedings of a Technical Committee Meeting of jointly organized by International Atomic Energy Agency and the Nuclear Energy Agency of the OECD, 26-29 August, Vienna, 13-22p.

Taşköprü, C., Özden, S., Günay, O., Aközcan Pehlivanoğlu, S., Saç, M., İçhedef, M. 2024. Natural and artificial radioactivity levels and external radiation dose levels of sand samples collected from Lara Beach, Antalya, Türkiye. Journal of Radioanalytical and Nuclear Chemistry, 1-7. DOI: 10.1007/s10967-024-09608-1

Unluer, A. T., Kocaturk, H., Doner, Z., Kaya, M., Yıldırım, D. K., Kumral, M., Özdamar, Ş. 2021. Geyikli (Çanakkale, Turkey) Heavy Mineral Sands: Insights to Their Origin Related with Alkaline Intrusive Rocks. Bitlis Eren University Journal of Science and Technology, 11(1), 13-16. DOI: 10.17678/beuscitech.900036

UNSCEAR, 2000. United Nations Scientific Committee on the effects of atomic radiation, sources and effects of ionizing radiation. Report to General Assembly, with Scientific Annexes United Nations. United Nations, New York.

Veiga, R., Sanches, N., Anjos, R. M., Macario, K., Bastos, J., Iguatemy, M., ... Umisedo, N. K. 2006. Measurement of natural radioactivity in Brazilian beach sands. Radiation measurements, 41(2), 189-196. DOI: 10.1016/j.radmeas.2005.05.001

Washington, H. S. 1899. The Petrographical Province of Essex County, Mass. II. The Journal of Geology, 7(1), 53-64.

Yalcin, M. G., Unal, S. 2018. Natural radioactivity levels and associated radiation hazards in ophiolites around Tekirova, Kemer, and Kumluca Touristic Regions in Antalya, Turkey. Journal of Radioanalytical and Nuclear Chemistry, 316, 321-330. DOI: 10.1007/s10967-018-5760-1

Yiğitbaş, E., Şengün, F., Tunç, İ.O., 2014. Biga Yarımadası'nda (KB Anadolu) Neojen Öncesi Tektonik Birlikler ve Bölgenin Jeodinamik Evrimine Yeni Bir Bakış, TÜBİTAK ÇAYDAG-110Y281 Nolu Proje Raporu.

Yiğitbaş, E., Tunç, I. 2020. Pre-cambrian metamorphic rocks of the Sakarya Zone in the Biga Peninsula; late Ediacaran Gondwanaland active continental margin. Geological Bulletin of Turkey, 63(3). DOI: 10.25288/tjb.589144